TRPV3 channel activity helps cortical neurons stay active during fever.

Yiming Shen[1], Richárd Fiáth[2], Baskar Mohana Krishnan[1], István Ulbert[2,3,4], Michelle W. Antoine[1,5]*

[1]*Section on Neural Circuits, National Institute of Alcohol Abuse and Alcoholism, National Institutes of Health, Bethesda, MD 20892, USA.*

[2] *Institute of Cognitive Neuroscience and Psychology, HUN-REN Research Centre for Natural Sciences, Budapest, Hungary*.

[3]*Faculty of Information Technology and Bionics, Pázmány Péter Catholic University, Budapest, Hungary*

[4]*Center of Neurosurgery and Neurointervention, Semmelweis University, Budapest, Hungary*

[5] Lead contact

*Correspondence and requests for materials should be addressed to: michelle.antoine@nih.gov (M.W.A).

Conflict of interest statement: The authors declare no competing financial interests.

Abstract

Fever raises body temperature (T_b) from ~37 °C to beyond 38.4 °C to combat pathogens. While generally well tolerated below 40 °C, in rare cases fever can abnormally elevate neural activity and induce seizures in neurotypical children aged 2–5 years. This study investigates the mechanisms by which neuronal activity is maintained and stabilized during exposure to fever-range temperatures. Recordings of layer (L)4-evoked spiking in L2/3 pyramidal neurons (PNs) of mouse somatosensory cortex revealed four outcomes as temperature increased from 30°C to 36 °C and 39 °C (fever-range): neurons remained inactive, stayed active, ceased activity, or initiated activity. Roughly equal proportions of neurons ceased or initiated spiking, making the subset of "STAY" PNs, those that remain active across temperatures, crucial for maintaining stable cortical output. STAY PNs were more prevalent at younger postnatal ages. Their firing stability was supported by a distinct ion channel composition, including the thermosensitive channel TRPV3, which enables continued spiking by adjusting depolarization to meet spike threshold. Intracellular blockade of TRPV3, but not TRPV4, significantly reduced the proportion of STAY PNs and suppressed spiking at 39 °C. Moreover, in *Trpv3*$^{-/-}$ mice, temperature increases to 39 °C reduced both spiking and postsynaptic potential amplitude, and these mice exhibited a delayed seizure onset. Together, these findings suggest that TRPV3 contributes to the preservation of cortical activity during fever.

Keywords: development; TRPV3 channel; TRPV4 channel; fever; temperature; seizures; network stability.

Introduction

In most mammals, including humans, core body temperature (T_b) is tightly regulated between 36.1 and 37.8°C, with a daily fluctuation of 0.5°C (Campbell I, 2008). Fever or other thermal challenges can impede heat dissipation to significantly increase T_b beyond 38°C (Wang et al., 2014). Because global brain temperature and core body temperature are largely congruent, large increases in temperature affect both regions (Wang et al., 2014). Increases in body temperature up to 40 °C are generally well tolerated, but temperatures above 42 °C (within the hyperthermia and heat stress range) become harmful, leading to protein denaturation and cell death. The body and brain employ protective mechanisms, such as heat shock proteins, to cope with heat stress. These proteins are rapidly induced or upregulated at noxious temperatures, aiding in the refolding or degradation of damaged proteins once temperatures return to physiological levels (Miller and Fort, 2018). However, the mechanisms that stabilize and preserve neuronal firing at lower, fever-range temperatures are not well understood.

In rare cases, moderate-grade fevers (T_b = 38.1 to 39°C) cause seizures in children aged 6 months to 6 years, with the highest susceptibility between 2 and 5 years (Oakley et al., 2009, Shinnar and O'Dell, 2004). A seizure is defined as a sudden, temporary burst of synchronized, excessive neuronal firing in the brain. These febrile seizures (FS) are almost typically triggered by the thermal component of fever, as infections or metabolic disorders are absent (Shinnar and O'Dell, 2004). Additionally, FS can be induced solely by increased T_b due to ambient heat, such as a warm bath, hot room, or overdressing. Beyond age five, FS rarely occur, suggesting that developmental changes in brain physiology stabilize network excitability during this window of susceptibility (Shinnar and O'Dell, 2004). Identifying the electrophysiological mechanisms underlying this protective shift could provide insight into normal brain maturation and reveal processes whose disruption may increase susceptibility to febrile seizures.

Rodents exhibit a similar age-dependent susceptibility to thermally induced seizures. The second postnatal week is proposed as a developmental window of heightened seizure susceptibility. During this period, fever-range temperatures (38.1 to 39°C), comparable to the range at which FSs occur in children (Holtzman et al., 1981), do not typically induce seizures. Instead, seizures arise only at higher thresholds (> 42.7 °C), consistent with hyperthermic rather than febrile seizures. This raises the question: what physiological changes occur during the second postnatal week that prevent seizures from being triggered at fever-range temperatures (~ 39°C)?

For practical reasons, EEG recordings for the onset of FS in humans are limited. However, EEG traces from rodents with thermally induced seizures show that ictal events often initiate in the hippocampus and propagate to the cortex, with the later spread to the cortex being correlated to the more severe behavioral stages of the seizure i.e. Racine stage > 4 (Dube et al., 2010; Baram et al., 1997). Thus, the cortex represents a critical locus in the seizure phenotype and likely contains mechanisms that may alter neural activity in response to temperature changes. In this manuscript, rather than examining how fever provokes seizures, we focus on identifying the electrophysiological adaptations during postnatal development that stabilize cortical activity at 39°C. Specifically, we compare two developmental stages flanking the proposed window of hyperthermic seizure susceptibility (P12–14): an earlier stage (P7–8) and a later stage (P20–23). This design also provides negative controls, allowing us to determine whether changes observed in the P12–14 window are unique.

Early comparative studies correlating rat and human brain development using neuronal birth dates, myelination patterns, and saltatory growth stages, suggest that 5–7-day-old rats approximate full-term human newborns (Dobbing and Sands, 1973). More recent analyses based on hippocampal and cortical maturation indicate that the second postnatal week (P10–

106 14) corresponds to human infancy (Baram et al., 1997; Bender et al., 2004). In contrast, the
107 third and fourth postnatal weeks align with the human juvenile stage (Baram et al., 1997). Here,
108 using wildtype mice across three postnatal developmental periods—postnatal day (P)7-8
109 (newborn), P12-14 (infancy), and P20-26 (juvenile)—we investigated the electrophysiological
110 properties, *ex vivo* and *in vivo*, that enable excitatory cortical pyramidal neurons (PNs) neurons
111 in mouse primary somatosensory (S1) cortex to remain active during temperature increases
112 from 30°C (standard in electrophysiology studies) to 36°C (physiological temperature), and then
113 to 39°C (fever-range).

114

115 Finally, to begin identifying molecular determinants that may mediate the electrophysiological
116 properties enabling firing stability in cortical PNs, we extended our studies to two members of
117 the thermosensitive, Ca^{2+}-permeable, nonselective cation channels of the transient receptor
118 potential vanilloid (TRPV) family: TRPV3 and TRPV4. These channels are activated within the
119 innocuous warm temperature range (TRPV3: 31–39 °C; TRPV4: 27–34 °C) (Su et al., 2023;
120 Shibasaki et al., 2007), unlike TRPV1 and TRPV2, which respond to noxious heat above 42 °C
121 and 52 °C, respectively (Kasho and Tominaga, 2022). TRPV3 and TRPV4 share low (~41%)
122 amino acid sequence identity (Smith et al., 2002) and are both expressed in the brain (Xu et al.,
123 2002; Caterina, 2007; Kanju et al., 2016; Chen et al., 2022). Given its activation within the 31–
124 39 °C range, we hypothesized that TRPV3 may specifically contribute to neuronal adaptations
125 occurring within fever range (Su et al., 2023; Shibasaki et al., 2007).

126

127 In summary, we aimed to elucidate adaptative neural mechanisms that allow cortical excitatory
128 PNs to maintain stable spiking despite substantial increases in brain temperature into the fever
129 range. Across three postnatal developmental ages, excitatory cortical PNs responded to
130 depolarizing stimuli during temperature increases from 30°C to 39°C, by remaining inactive,

131 continuing to spike, ceasing spiking, or initiating spiking. Nearly equal proportions of neurons
132 ceased or initiated activity, so overall firing stability was maintained largely by “STAY” neurons,
133 which remained active throughout temperature increases. We propose that STAY neurons likely
134 achieve this stability through unique ion channel compositions, including those from TRPV3,
135 which allows for higher depolarization levels through increased excitatory synaptic input relative
136 to inhibitory input.

137

138 **Results**

139 **Body Temperature rises to fever levels during regular activity and exposure to higher**
140 **ambient temperatures.**

141 Contrary to common belief, T_b is not fixed but varies with arousal state, motor activity, and
142 environmental temperature (Kiyatkin EA, 2019; Hankenson et al., 2018**;** Wang et al., 2014).
143 Using a sterile IPTT-300 implantable temperature transponder (Bio Medic Data Systems, LLC)
144 with a 0.025-second time constant and 0.1°C accuracy, T_b measurements were recorded every
145 five-minutes over six hours from 2–3-week-old wildtype mice in an open-field arena at room
146 temperature (**Figure 1A**). This analysis revealed a stable median temperature of 36.5°C with a
147 maximum and minimum fluctuation of 0.5°C (**Figure 1A**). However, within-subject analysis
148 showed brief T_b elevations into the fever range (shaded red bars) during increased activity like
149 cage climbing or digging (**Figure 1B-C**). Exposure to infrared light elevates ambient
150 temperatures and induces prolonged T_b elevations into the fever range, with an onset within
151 minutes and a duration of several hours (**Figure 1D**).

152

153 **Spiking in P12-P14 cortical excitatory pyramidal neurons remains stable as temperature**
154 **enters the fever range.**

155 To investigate how postnatal cortical neurons respond to fever-range temperature, we used
156 whole-cell current clamp electrophysiology to record natural spiking, evoked synaptically, as
157 brain slice temperature gradually rose from 30°C to 36°C to 39°C in PNs (**Figure 2A-B**). Acute
158 S1 cortex slices (350 μm thick) were prepared using standard methods (Antoine et al., 2019).
159 PNs were visually identified via infrared DIC optics, and physiological verification for regular
160 spiking was done in current clamp. Neuronal activity in PNs was evoked by stimulating in the
161 barrel center of cortical layer (L) 4 using a bipolar electrode (0.2 ms pulses) at a specific
162 stimulation intensity i.e. 1.4X Eθ (**Figure 2A**). Eθ is defined as the minimal intensity evoking an
163 excitatory postsynaptic current (EPSC) during more than 3 of 5 consecutive sweeps with 10 s
164 inter-sweep interval. Eθ was determined in voltage clamp for each recorded cell, prior to
165 recording post-synaptic potentials (PSPs) and spiking in current clamp. L4- evoked PSPs and
166 spiking, were recorded from L2/3 PNs, with resting membrane potential (V_m) set just below
167 spike threshold (-50mV) to simulate in vivo conditions (Yamashita et al., 2013).
168
169 Recordings of synaptically-evoked activity in L2/3 wildtype cortical excitatory PNs from P12-14
170 mice showed significant effects of temperature elevations from 30°C to 39°C. These changes
171 resulted in an increased depolarization required to reach spike threshold (ST) (defined as the
172 minimal V_m that just elicits spiking) (**Figure 2B-C**). Consistent with previous findings,
173 measurements of input resistance (R_{in}) which reflect the extent to which membrane channels
174 are open, showed significant reductions across all recorded neurons with increasing
175 temperature (**Figure 2D**). Similar temperature-induced effects on R_{in} have been reported in L2/3
176 PNs in the rat visual cortex (Hardingham and Larkman, 1997) and in hippocampal CA1 and CA3
177 PNs from P13-P16 mice (Kim and Connors, 2012). The depolarized ST and reduced R_{in} in PNs
178 would likely decrease cell excitability and spiking. Indeed, the percentage of spiking cells
179 decreased during temperature elevations from 30°C to 39°C (**Figure 2E**). However, contrary to
180 expectations, average spiking remained remarkably stable (**Figure 2F-G**). We also examined

181 the temperature-induced effects on L2/3 PNs in the absence of excitatory and inhibitory synaptic
182 inputs. Intrinsic spiking was measured in the presence of synaptic blockers (100 μM APV, 10
183 μM NBQX, and 3 μM gabazine). PNs were held at -80 mV, followed by positive current injection
184 (500 ms) steps to determine rheobase (the minimum current injection needed to produce one
185 spike). At 39°C, rheobase was increased compared to 30°C (**Figure 2H**). Current was injected
186 up to 250 pA above rheobase at 30°C, 36°C, and 39°C, using a new brain slice for each
187 recording. Although rheobase was decreased at 39°C compared to 30°C, we found that the
188 mean number of spikes produced did not differ across current steps (**Figure 2I**).
189

190 **Spiking in P7-8 cortical excitatory pyramidal neurons decreases as temperature enters**
191 **the fever range.**

192 This stability in average spiking at 39°C, despite the loss of some previously active neurons,
193 suggests the presence of temperature-adaptive changes in PNs that help to maintain normal
194 circuit activity levels. These changes may either initiate firing in previously non-spiking neurons
195 or either maintain or elevate spiking levels in currently active cells. Interestingly, in P7–8 mice,
196 temperature elevations from 30 °C to 39 °C produced effects on ST and R_{in} similar to those
197 observed in P12–14 mice, with ST increasing and R_{in} decreasing (**Figure 3A–D**). However, in
198 P7-8 PNs, during temperature elevations from 36 to 39°C, ST did not increase, and R_{in}
199 decreased (**Figure 3C-D**). Additionally, the percentage of spiking PNs decreased during
200 temperature elevations from 30°C to 39°C (**Figure 3E**). In contrast to P12-14 PNs, the average
201 spiking levels in P7-8 PNs significantly decreased during these temperature elevations (**Figure**
202 **3F-G**). This suggests that temperature-adaptive changes, possibly involving R_{in} and ST, which
203 help maintain average spiking levels at fever temperatures despite the loss of some previously
204 active neurons, may be underdeveloped or absent at this earlier age.
205

206 **Increased depolarization at higher spike thresholds helps maintain stable spiking activity**
207 **in cortical pyramidal neurons during temperature elevations.**
208 The temperature-induced increases in ST at P12-14, would make it harder for a cell to spike, as
209 larger depolarization levels would be required to maintain spiking (**Figure 4A**). Therefore, we
210 hypothesized that in cells with increased ST that remain spiking, a temperature-adaptive change
211 might involve a proportional increase in depolarization. To determine if larger depolarizations
212 were associated with higher (less negative) STs, we analyzed the relationship between peak
213 postsynaptic potential (PSP), which indicates maximum depolarization, and ST (**Figure 4B**).
214 Correlation analysis revealed a strong positive correlation between peak PSP and spike
215 threshold at P12-14, which was absent at P7-8 and P20-23 (**Figure 4C**). This correlation was
216 specific to these parameters, as it did not occur for comparisons involving input resistance, an
217 intrinsic property which is affected by temperature changes (**Figure 4D-E**).
218
219 One mechanism that could promote enhanced depolarization is a reduction in the inhibitory PSP
220 (IPSP) (**Figure 4F**). In addition to the early component of the PSP (the peak), where excitation
221 is maximal, we also quantified the late component, where inhibition levels are greatest and thus
222 largely represents the IPSP (Bhatia et al., 2019; Antoine et al., 2019) (**Figure 4B**). This analysis
223 revealed that the late PSP (LPSP) was significantly reduced with temperature elevations from
224 30°C to 39°C (**Figure 4G**). Further analysis indicated that there was no correlation between the
225 ST and LPSP at any age (P7-8: r=0.17, P=0.41, XY pairs=25; P12-14: r=0.24, P=0.31, XY
226 pairs=19; P20-23: r=0.33, P=0.28, XY pairs=13 Pearson's test). However, a significant,
227 moderate relationship occurred between the magnitude of the LPSP and the PSP threshold
228 (**Figure 4H**). Thus, PNs with increased STs and larger PSPs were part of a circuit where
229 synaptic inhibition was reduced across all or most PNs, regardless of whether STs were
230 elevated. These results suggest that at P12-14, ST is sensitive to temperature increases and
231 spiking is maintained by larger depolarization levels in these neurons.

232

233 **Cortical excitatory neurons that remain active at febrile temperatures exhibit increased**
234 **spiking rates.**

235 At a later age (P24-P26), we applied external heat to elevate normal T_b (36°C) into the fever
236 range and used *in vivo* high-density, extracellular electrophysiological recordings to capture
237 single-unit activity in the S1 cortex of ketamine/xylazine anesthetized wildtype mice (**Figure 5A**).
238 Unlike in vitro whole-cell patch-clamp recordings, extracellular recordings allow analysis only
239 from cells that spike throughout the recording period during temperature elevations from 36°C
240 (baseline) to fever-range. This is largely due to the inability of spike sorting algorithms to reliably
241 track neurons that stop firing during the recording.

242

243 Color maps (with yellow and red indicating spiking activity) illustrate multiunit activity obtained in
244 the left and right cortices during baseline temperature (left), warming to fever T_b (middle), and
245 cooling back to 36°C (recovery upon heat removal) are shown in **Figure 5B**. **Figure**
246 **5C** presents example traces of spiking activity recorded from three cortical positions (marked by
247 black, gray, and white asterisks on the right side of panels in figure **5B**). Following manual
248 curation, single units (n = 633) were classified as putative inhibitory interneurons or excitatory
249 pyramidal neurons (PNs) based on their spike waveform duration (Barthó et al., 2004; see
250 Methods). The spike duration was calculated as the time difference between the trough and the
251 subsequent waveform peak of the mean filtered (300 – 6000 Hz bandpassed) spike waveform.
252 Durations of extracellularly recorded spikes showed a bimodal distribution (Hartigan's dip test;
253 $p < 0.001$) characteristic of the neocortex with shorter durations corresponding to putative
254 interneurons (narrow spikes) and longer durations to putative principal cells (wide spikes). Next,
255 k-means clustering was used to separate the single units into these two groups, which resulted
256 in 140 interneurons (spike duration < 0.6 ms) and 493 principal cells (spike duration > 0.6 ms),
257 corresponding to a typical 22% - 78% (interneuron – principal) cell ratio. **Figure 5D** displays

258 representative single units isolated via spike sorting, with unit 3 representing a putative
259 interneuron.
260
261 Finally, the firing rates of neurons were computed separately during the three distinguished
262 periods (baseline, thermal fever (39°C) and recovery back to 36°C). To decrease the effect of
263 transient changes (e.g., tissue recovery during the baseline period or the short-term effect of
264 heating during the thermal fever period), for each 45-minute-long period, we used only the last
265 25-minutes to calculate the mean firing rates of neurons. The normalized average firing rate for
266 each animal (n= 5) was calculated for these putative inhibitory interneurons and excitatory PNs
267 across the recording session. We found that *in vivo*, putative excitatory PNs that remained
268 active increased their spike rates at fever temperatures (**Figure 5E**). The normalized firing rates
269 of five representative units are shown in **Figure 5F** during the baseline, warming (red shaded
270 area), and recovery periods. Additionally, we observed that putative inhibitory interneurons that
271 remained active also increased their spike rates at fever temperatures (**Figure 5E**).
272
273 Consistent with these *in vivo* findings, *ex vivo* recordings at a similar age (P20-23) showed that
274 11.1% of recorded excitatory PNs (n=27 cells) spiked at both 36°C and 39°C (Figure 5G).
275 However, similar to the *in vivo* condition, neurons that remained spiking at 36°C and 39°C
276 increased their spike/firing rate (**Figure 5H**). Along with the 11.1% of recorded excitatory PNs
277 that stayed spiking during temperature increases from 36°C to 39°C, roughly equal proportions
278 of neurons stopped spiking and started spiking (**Figure 5G**). Thus, neurons that maintain
279 spiking at fever temperatures play a crucial role in determining the overall activity levels of the
280 circuit. Additionally, we found that the proportion of PNs that remain spiking from 36°C to 39°C
281 is higher at earlier ages (P12-14) compared to later ages (P20-23) (**Figure 5I**).
282

Excitatory pyramidal neurons that remain spiking with temperature elevations into fever range exhibit unique intrinsic properties.

As neurons that remain spiking with temperature elevations may be crucial in setting overall cortical circuit activity levels, we sought to uncover additional information about the intrinsic characteristics of cortical PNs at P12-14 that facilitate their activity at 36°C to 39°C. We refer to neurons that retained spiking at all three temperatures (30°C, 36°C, and 39°C) as STAY neurons, while those cells that stopped spiking upon temperature transitions from 30°C to 36°C or 36°C to 39°C are denoted as STOP neurons. Firstly, in STOP and STAY neurons, ST increased during temperature elevations from 30°C to 39°C (**Figure 6A**). However, in STOP PNs, the increases in ST were greater than in those neurons that continued spiking (**Figure 6A**). The ST of neurons that continued spiking at 39°C was similar in magnitude to that of neurons that stopped spiking at 36°C.

There was an interaction of temperature and whether the PNs were STOP or STAY cells in the PSP (P=0.048, two-way ANOVA, mixed-effects model), with a trend toward larger PSPs in the STAY PNs (**Figure 6B**). STAY cells showed a strong positive correlation between PSP and ST (**Figure 6C-D**). At 30°C, STAY neurons had larger LPSPs (**Figure 6E**). However, inhibition levels in these PNs were unique in that inhibition levels significantly decreased with temperature elevations (**Figure 6E**). Moreover, we found a significant moderate inverse correlation between ST and LPSP in the STAY cells that remain spiking at 39°C (r=-0.57, P=0.046, XY pairs=13, Spearman). Thus, in PNs that stay spiking, the excitation and inhibition levels are matched to facilitate greater depolarization and maintain spiking activity. Temperature-induced alterations in spike height and spike afterhyperpolarization (AHP) were not different between STAY and STOP cells, while R_{in} was largely insensitive to temperature changes in STAY PNs but not in STOP PNs (**Figure 6F-H**).

309 **Temperature elevations in the fever range increase TRPV3 currents in cortical pyramidal**
310 **neurons.**
311 Next, we sought to identify molecular determinants that might underlie the properties of STAY
312 cells. We focused on the transient receptor potential vanilloid 1-4 (TRPV1-4) channels, a family
313 of thermosensitive, Ca^{2+}-permeable, nonselective cation channels. Of these, only TRPV3 and
314 TRPV4 are activated within the innocuous warm temperature range (31-39°C), whereas TRPV1
315 and TRPV2 respond to noxious heat above 42°C and 52°C, respectively (Kasho and Tominaga,
316 2022). TRPV3, in particular, has a reported temperature threshold for activation between 31–
317 39°C, with Smith et al., 2002 noting activation at 39°C.
318
319 We examined TRPV3 protein expression by immunohistochemical staining at P7, P14, and P21
320 (**Figure 7A-B**). Staining specificity was confirmed at all ages by co-incubating the TRPV3
321 antibody with a TRPV3 blocking peptide, with an example shown for a P7 brain section (**Figure**
322 **7A**, right panel). TRPV3 expression was detected in S1 cortex at all ages, with strong
323 expression in L2/3 at P14 but not at P7 or P21 (**Figure 7A**). Outside S1 cortex, TRPV3 was also
324 present in the hippocampus, thalamus, and striatum (**Figure 7A-B**). Co- immunostaining for
325 TRPV4 revealed several brain regions where TRPV4 (red color) and TRPV3 (green color) were
326 non-overlapping (**Figure 7B, top-left panel**). In the S1 cortex at P14, TRPV3 was detected in
327 L4 barrels and showed a patchy distribution in L2/3, with some patches displaying more intense
328 staining (**Figure 7B, bottom-right panel**). This pattern was not observed for TRPV4 (**Figure**
329 **7B, bottom-left panel**).
330
331 Using whole-cell voltage clamp, we recorded TRPV3 currents at different voltages in cortical
332 excitatory PNs with bath application of camphor (5 mM), a TRPV3 agonist (Moqrich et al., 2005)
333 (**Figure 8A**). We observed a significant increase in TRPV3 currents at 39°C (**Figure 8B-C**, two-
334 way repeated measures ANOVA, with Fisher's LCD test). We also measured the net TRPV3

335 currents by comparing TRPV3 current densities recorded in the absence and presence of
336 forsythoside B, a natural TRPV3 inhibitor found in the plant *Lamiophlomis rotate* with an IC 50 of
337 6.7 μmol/L and no obvious inhibitory effects on the other TRPV channels like TRPV1 or 4
338 (Zhang et al., 2019). Consistent with Smith et al., 2002, who noted TRPV3 activation at 39°C,
339 we also observed a net positive TRPV3 current at 39°C (**Figure 8D-G**).
340

341 **Inhibiting TRPV3, but not TRPV4 channels, significantly reduced the population of STAY**
342 **pyramidal neurons and spiking levels at fever temperature.**

343 To investigate the potential role of TRPV3 and TRPV4 in regulating STAY PN phenotype in the
344 S1 cortex during temperature increases from 30-39°C, we applied the following blockers:
345 forsythoside B (50μM) or RN1734 (10μM, TRPV4 blocker) intracellularly in our recordings of L4-
346 evoked spiking at 1.4X Eθ in L2/3 PNs (**Figure 9A**). RN1734 is a highly selective antagonist for
347 TRPV4 with an IC 50 of 5.9 μmol/L and minimal to negligible affinity for the other TRPV
348 channels (Vincent et al., 2009). These blockers phenocopy electrophysiological effects
349 observed in *Trpv4* $^{-/-}$ *KO* and *Trpv3* $^{-/-}$ *KO* mice (Chen et al., 2022). For instance, *Trpv3* $^{-/-}$ *KO*
350 mice exhibit a hyperpolarizing effect on the resting membrane potential (RMP) in striatal MSNs
351 and L2 stellate neurons in the entorhinal cortex (Chen et al., 2022). This hyperpolarization
352 reflects reduced TRPV3 activity, which normally promotes cation influx (Shibasaki et al., 2007;
353 Chen et al., 2022). Although increases in temperature alone can depolarize the RMP, consistent
354 with prior reports in *Trpv3* $^{-/-}$ mice, our recordings of L4-evoked spiking in L2/3 PNs of S1 cortex
355 showed a similar trend toward RMP hyperpolarization with intracellular TRPV3 block via
356 forsythoside at 30 °C and 36 °C, and a significant enhancement at 39°C. Specifically, in the
357 absence of block (n = 13 cells) versus with TRPV3 blocker (n = 15 cells), the RMP values were:
358 30 °C: −75.1 ± 1.1 vs. −77.1 ± 1.0 mV (P = 0.273); 36 °C: −73.5 ± 1.2 vs. −76.3 ± 1.1 mV (P =

359 0.273); 39 °C: −71.3 ± 1.0 vs. −74.4 ± 1.1 mV (P = 0.048); two-way repeated-measures ANOVA
360 with Fisher's LSD test.

361

362 Furthermore, we found that intracellular blockade of TRPV3 caused a significant reduction in the
363 percentage of STAY neurons (No block: 27% (37 recorded cells), TRPV3 block: 8% (n=26
364 recorded cells), TRPV4 block: 17% (n=24 recorded cells), two-tailed binomial test) (**Figure 9B**).
365 Consistent with the STAY cells being largely responsible for maintaining stable average spiking
366 during temperature elevations, spiking was reduced in PNs with intracellular TRPV3 blockade
367 during the temperature transitions from 30°C to 39°C **(Figure 9C**). TRPV3 block did not occlude
368 the increases in the depolarization required to reach ST (TRPV3 blocker: 30°C: 7.15 ± 0.57,
369 36°C: 8.39 ± 0.26, 39°C: 10.0 ± 0.94, 30°C vs 39°C: P=0.007, One- way repeated measures
370 ANOVA, mixed-effects model with Tukey's test). However, it did abolish the temperature
371 induced increases in the PSP (TRPV3 blocker: 30°C: 2.37 ± 0.36, 36°C: 2.45 ± 0.38, 39°C: 2.22
372 ± 0.25; No blocker: 30°C: 2.47 ± 0.32, 36°C: 2.90 ± 0.32, 39°C: 3.32 ± 0.52 , 30 vs 39°C:
373 P=0.030, One-way repeated measures ANOVA, mixed-effects model with Dunnett's test).
374 Consistently, TRPV3 block abolished the positive correlation between ST and PSP (No block:
375 XY pairs=27, TRPV3 blocker: XY pairs=18, Pearson's test) (**Figure 9D**).

376

377 Furthermore, in keeping with the correlation between the magnitude of the LPSP and the PSP
378 threshold, we found that TRPV3 blockade also prevented the temperature induced decreases in
379 the LPSP (**Figure 9E**). Moreover, these reductions in spiking with TRPV3 blockade were not
380 dependent on temperature-induced decreases in R_{in}, as changes to PNs were similar in the
381 TRPV3 block and no-block conditions (**Figure 9F**). Altogether, these results suggest that
382 TRPV3 expression or its functional effects—such as mediating Ca^{2+} or other cation (Na^{+}, K^{+})
383 influx to promote increased depolarization with spike threshold increases—may define the

384 subset of STAY neurons. Given this role, the loss of TRPV3 is expected to promote
385 temperature-induced hypoactivity in cortical circuits rather than exacerbate seizure activity.
386
387 **TRPV3 knockout mice exhibit reduced spiking activity at febrile temperatures and**
388 **delayed seizure onset.**

389 Recordings of L4-evoked PSPs and spiking in L2/3 cortical PNs from wildtype (WT) and
390 homozygous *Trpv3* knockout (*Trpv3*$^{-/-}$) (Moussaieff A et al., 2008) mice revealed similar degrees
391 of temperature sensitivity in ST and R_{in}. Febrile temperatures increased ST and decreased R_{in}
392 (**Figure 10A-C**). Consistent with findings that TRPV3 blockade using 50μM forsythoside B
393 reduces spiking in cortical L2/3 PNs, we observed significantly reduced spiking in *Trpv3*$^{-/-}$ mice
394 as well (**Figure 10D**). Analysis of postsynaptic potentials in these neurons, showed that, in WT
395 mice, PSP amplitude increased with temperature elevation into the febrile range, whereas this
396 temperature-dependent depolarization was absent in *Trpv3*$^{-/-}$ mice (**Figure 10E**). This reduction
397 in spiking is consistent with the idea that, during increases in STs, concurrent increases in PSP
398 amplitude help sustain neuronal spiking. These findings support the conclusion that TRPV3
399 contributes to enhanced depolarization and excitability at febrile temperatures.

400 We next examined the effects of reduced *Trpv3* expression on hyperthermia-induced seizures in
401 WT(*Trpv3*$^{+/+}$), heterozygous (*Trpv3*$^{+/-}$), and homozygous knockout (*Trpv3*$^{-/-}$) P12 pups. As
402 described in **figure1D**, mice were exposed to infrared light to raise their core T_b into the range of
403 hyperthermia (>40°C; **Figure 10F**). To enable wireless, non-invasive T_b recordings, all mice
404 were implanted with temperature transponders. Baseline T_b measurements prior to infrared
405 exposure revealed no significant differences across genotypes (*Trpv3*$^{+/+}$: 33.7 ± 0.44°C, *Trpv3*$^{+/-}$
406 : 33.7 ± 0.33°C, *Trpv3*$^{-/-}$: 32.8 ± 0.10°C; One-way ANOVA with Tukey's multiple comparison
407 test, $F(2,11) = 2.41$, $P = 0.136$)). As T_b increased during infrared exposure, P12 mice typically
408 transitioned from rest to active walking and exploratory behavior. The T_b at which mice became

409 ambulatory did not significantly differ across genotypes (*Trpv3*$^{+/+}$: 37.5 ± 0.55°C, *Trpv3*$^{+/-}$: 36.3
410 ± 0.43°C, *Trpv3*$^{-/-}$: 36.6 ± 0.34°C; One-way ANOVA with Tukey's multiple comparison test,
411 F(2,11) = 1.34, P = 0.301).

412 As T_b reached 41–42°C, mice exhibited loss of postural control (LPC), defined as collapse and
413 failure to maintain upright posture. LPC is a key behavioral marker of cortical and motor circuit
414 dysfunction. The T_b at which LPC occurred was significantly lower in *Trpv3*$^{-/-}$ mice compared to
415 wildtype controls (**Figure 10G**). LPC was followed by the rapid onset of generalized seizures.
416 While the T_b at seizure onset was not significantly different among genotypes (**Figure 10H**), the
417 time to seizure onset was significantly prolonged in both *Trpv3*$^{+/-}$ and *Trpv3*$^{-/-}$ mice. Specifically,
418 *Trpv3*$^{+/-}$ mice exhibited a 49.4% increase, and *Trpv3*$^{-/-}$ mice a 91% increase in latency to seizure
419 compared to WT mice (**Figure 10I**). Importantly, the rate of T_b increase leading to seizure did
420 not differ across genotypes (*Trpv3*$^{+/+}$: 0.011 ± 0.003°C/s, *Trpv3*$^{+/-}$: 0.013 ± 0.002°C/s, *Trpv3*$^{-/-}$:
421 0.012 ± 0.001°C/s; One-way ANOVA with Tukey's multiple comparison test, F(2,11) = 0.1055, P
422 = 0.9008), suggesting the delayed seizure onset was not due to slower heating. Together, these
423 findings indicate that reduced TRPV3 function increases resistance to seizure initiation and/or
424 propagation under febrile conditions, likely by decreasing neuronal excitability.

425 **Discussion**

426 In this study, we aimed to elucidate adaptive neural mechanisms that enable excitatory PNs to
427 remain active despite substantial increases in brain temperature into the fever range. Our
428 electrophysiological assessments across three postnatal ages, P7-8, P12-14 and P20-23
429 showed that excitatory PNs responded to temperature increases from 30°C to 39°C by either
430 remaining inactive, staying active, ceasing activity, or initiating activity. Roughly equal portions
431 of neurons ceased or initiated activity, so firing stability was largely maintained by those that
432 remained active, i.e., STAY neurons. The overall proportion of PNs that remain spiking from
433 36°C to 39°C was higher at P12-14 compared to P20-23. This increased proportion at earlier

434 ages could potentially reflect the increased risk for febrile seizure occurrence at earlier postnatal
435 ages.
436
437 STAY neurons likely possess a unique composition of ion channels that enable them to exhibit
438 temperature sensitivity in spike threshold but not in input resistance, and adjust their
439 depolarization levels to match the ST value. Our initial characterization focused on *Trpv3* and
440 *Trpv4*, two members of a family of thermosensitive transient receptor potential vanilloid
441 channels that are expressed in the brain and activated between 30-39°C, the temperature range
442 of our study. Intracellular blockade of TRPV3, but not TRPV4, significantly decreased the
443 population of STAY PNs and prevented stability in spiking activity during temperature increases
444 into fever range.
445
446 TRPV3 is highly expressed in various tissues, including epithelial cells of the skin and
447 oropharynx, the tongue, testis, dorsal root ganglion, trigeminal ganglion, spinal cord and brain
448 (Moussaieff A et al., 2008 and Xu et al., 2002). It plays a crucial role in skin and hair generation
449 as well as in the perception of pain and warmth on the skin. However, its role in the central
450 nervous system remains to be further elucidated. In the brain, TRPV3 is expressed in several
451 neuronal types, including cortical and striatal neurons (Xu et al., 2002; Chen et al., 2022).
452 TRPV3 has a reported temperature threshold for activation between 31–39°C, with Smith et al.,
453 2002 noting activation at 39°C. Consistent with this, we observed the strongest physiological
454 effects in cortical PNs at 39°C. At this temperature, intracellular blockade of TRPV3 reduced
455 average spiking levels and temperature-induced increases in the PSP. Additionally, a potential
456 early postnatal temperature-dependent activity mechanism in PNs, where levels of excitatory
457 and inhibitory input are adjusted to match the cell's ST, was abolished with TRPV3 blockade.
458 Altogether, these results suggest that TRPV3 blockade reduces net activity in sensory cortical
459 circuits by decreasing activity in STAY cells.

460

461 Although, TRPV3 channels are cation-nonselective, they exhibit high permeability to Ca^{2+} (
462 $Ca^{2+}>Na^{+}\approx K^{+}\approx Cs^{+}$) with permeability ratios (relative to Na^{+}) of 12.1, 0.9, 0.9, 0.9 (Xu et al.,
463 2002). Opening of TRPV3 channels activates a nonselective cationic conductance and elevates
464 membrane depolarization, which can increase the likelihood of generating action potentials.
465 Indeed, our observations of a loss of the temperature-induced increases in the PSP with TRPV3
466 blockade are consistent with a reduction in membrane depolarization. In S1 cortical circuits at
467 P12-14, STAY PNs appear to rely on a temperature-dependent activity mechanism, where
468 depolarization levels (mediated by higher excitatory input and lower inhibitory input) are scaled
469 to match the cell's ST. Thus, an inability to increase PSPs with temperature elevations prevents
470 PNs from reaching ST, so they cease spiking. See summary figure 11.
471

472 Previous research in *Trpv3* $^{-/-}$ KO mice revealed a similar phenotype of reduced activity with
473 diminished TRPV3 function (Chen et al., 2022). Whole-cell current-clamp recordings from
474 striatal MSNs and L2 stellate neurons in the entorhinal cortex at 36.5-37.5°C showed that
475 *Trpv3*$^{-/-}$ cells exhibited reduced intrinsic excitability, as evidenced by fewer spikes in response to
476 400-ms current steps, a hyperpolarized RMP, and a decrease in mEPSC frequency (Chen et al.,
477 2022). These electrophysiological effects were also replicated using pharmacological inhibition
478 of TRPV3 with 50 μmol/L forsythoside B (Chen et al., 2022). Additionally, consistent with the
479 idea that ischemic injury upregulates TRPV3 expression, leading to intracellular Ca^{2+} overload
480 and progressive cell death, inhibition of TRPV3, rather than N-methyl-D-aspartate (NMDA)
481 receptors, protected against progressive cell death after stroke (Chen et al., 2022).
482

483 As STAY PNs and neurons that initiate spiking at fever temperature ("START" cells) are active
484 at fever temperature, future research will focus on the molecular characterization of these cells

485 in the cortex and elsewhere in the brain at P12-14 and other ages. Interestingly, neurons that
486 initiate spiking at fever temperature are more prevalent at P20-23 than at the earlier ages
487 examined. TRPV4 block caused a subset of PNs to initiate spiking at 39°C, suggesting that low
488 TRPV4 expression could define the population of START cortical PNs, at least at P12-14.
489
490 Molecular characterization of STAY and START cell types may provide additional insights into
491 their function within normal brain circuits. In response to specific experiences, selective subsets
492 of neurons, known as "engrams," may become active to encode specific memories or
493 behavioral responses (Lee et al., 2021). Alternatively, neurons that become active could initiate
494 responses to specific stimuli, such as an increase in brain temperature. In this latter scenario,
495 these neurons may be part of the brain's homeostatic response to temperature increases, while
496 STAY neurons may play a critical role in facilitating ongoing (cognitive) functions during a fever.
497 Future research into the molecular characterization of these cell types could offer opportunities
498 to target and modulate their activity in a brain region-specific manner, potentially advancing
499 treatments for fever-associated seizures or epilepsies, such as Dravet Syndrome (a genetic
500 epilepsy typically initiating in early infancy) and febrile infection-related epilepsy syndrome
501 (FIRES).
502
503 **Acknowledgements**
504 This research was supported in part by the Intramural Research Program of the National
505 Institutes of Health (NIH). The contributions of the NIH authors were made as part of their
506 official duties as NIH federal employees, are in compliance with agency policy requirements,
507 and are considered Works of the United States Government. However, the findings and
508 conclusions presented in this paper are those of the authors and do not necessarily reflect the
509 views of the NIH or the U.S. Department of Health and Human Services. M.W.A. , R.F., and
510 Y.S., designed, performed, interpreted and analyzed physiology experiments. M.W.A., and Y.S.

designed, performed, and analyzed *ex vivo* electrophysiological experiments. R.F. designed, performed, and analyzed *in vivo* electrophysiological experiments. B.M.K. performed the immunohistochemistry for TRPV3 and TRPV4. M.W.A. wrote the paper. M.W.A and I.U. provided project supervision. We thank Dr. David Lovinger, Scientific Director of NIAAA, for his critical review of the manuscript. Research support was provided from the National Institute on Alcohol Abuse and Alcoholism (NIAAA) of the National Institutes of Health (NIH) under grant 1ZIAAA000440-02 (MWA) and the National Institute of Neurological Disorders and Stroke under grant 1K22NS105922-01 (MWA).

Materials and Methods

Animals

All experimental procedures were performed in accordance with the National Institutes of Health guidelines for care and use of laboratory animals and the EC Council Directive of September 22, 2010 (2010/63/EU). All experiments were approved by the Animal Care and Use Committee of the National Institute on Alcohol Abuse and Alcoholism (NIAAA) (Protocol # LIN-MA-1) and the Animal Care Committee of the HUN-REN Research Centre for Natural Sciences (RCNS) and by the National Food Chain Safety Office of Hungary (license number: PE/EA/1004-5/2021). Mice were housed under standard conditions with ad libitum access to food and water, under a 12-h light/dark cycle. The following mouse strains were obtained from The Jackson Laboratory (JAX):C57BL/6J (JAX 000664), FVB/N mice (JAX 004828), and Trpv3 **(**JAX 010773) (Moussaieff A et al., 2008; Moqrich et al., 2005). The day of birth was denoted as postnatal day (P)1. Both male and female mice were used for body temperature (T_b) recordings and electrophysiological experiments.

Body Temperature Measurements

537 All mice used for body temperature (T_b) recordings were implanted with sterile IPTT-300
538 Implantable Programmable Temperature transponders (Bio Medic Data Systems, LLC) at 2
539 weeks of age. The injection site was pre-cleaned with a betadine solution, and the sterile
540 transponders were injected subcutaneously using a pre-loaded 12-gauge syringe into animals
541 anesthetized with 4-5% isoflurane. The injection site was on the left side, approximately 11 mm
542 from the base of the hip, with the animal in the prone position. Post-implantation, the mice were
543 able to move, eat, and drink autonomously, with no adverse phenotypes noted. T_b recording
544 commenced at least 5 days after injection. Prior to recording, mice were brought into the
545 procedure room and allowed to habituate for 1 hour. T_b was recorded every 5 minutes for 6
546 hours using an IPTT-300 Implantable Programmable Temperature reader (DAS-8027) in a 37L
547 x 16W x 13H cm cage. T_b was recorded in the presence (**Figure 1D**) or absence (**Figure 1A-C**)
548 of infrared light. Infrared light exposure was provided via a 250-W temperature-controlled
549 infrared lamp (catalog #50320, Stoelting), set to 32.5-33.5 °C. The lamp was positioned ~15 cm
550 above the cage, and the ambient temperature was monitored every 5 minutes (**Figure 1D**).
551

552 **Slice Preparation**

553 Using standard methods, acute primary somatosensory cortex (S1) slices (350 µm thick) from
554 P7-8, P12-14, or P20-23 mice were cut in the "across-row" plane, oriented 35° toward coronal
555 from midsagittal (Antoine et al., 2019). The cutting solution contained (in mM): 85 NaCl, 75
556 sucrose, 25 D- (+)-glucose, 4 $MgSO_4$, 2.5 KCl, 1.25 NaH_2PO_4, 0.5 ascorbic acid, 25 $NaHCO_3$,
557 0.5 $CaCl_2$. Once cut, slices were transferred to a submerged-style holding chamber containing
558 standard Ringer's solution (in mM: 119 NaCl, 2.5 KCl, 1.3 $MgSO_4$, 1 NaH_2PO_4, 26.2 $NaHCO_3$,
559 11 D-(+)-glucose and 2.5 $CaCl_2$) and then incubated at 32°C for 30 minutes. Both solutions
560 were at neural pH (i.e., 7.3), 300 mOsm, and saturated with 95% O_2 and 5% CO_2. Slices were
561 kept at room temperature for at least 30 minutes before being transferred to a submerged
562 recording chamber.

563

564 *In Vitro* Physiology

565 Whole-cell current-clamp recordings were made from pyramidal neurons (PNs) visually
566 identified via infrared DIC optics. Physiological verification for regular spiking was done in
567 current clamp. Recordings were made using 3-6 MΩ micropipettes containing (in mM):116 K
568 gluconate, 20 HEPES, 6 KCl, 2 NaCl, 0.5 EGTA, 4MgATP, 0.3 NaGTP, 10 Na phosphocreatine,
569 with a Multiclamp 700B amplifier (Molecular Devices, Sunnyvale, CA). Where applicable,
570 forsythoside B (50 μM, TRPV3 blocker, Millipore Sigma Cat #: PHL83313) or RN1734 (10 μM,
571 *TRPV4 blocker*, Tocris Bioscience Cat #: 3746/25) was added to the internal solution. Camphor
572 (MedChem, Cat. No: HY-N0808) was added to the bath solution for experiments in **figure 8**.

573

574 Signals were filtered (2-6 kHz) and digitized (10-20 kHz). Perfusate temperature for all in vitro
575 experiments was regulated by a PC-connected Peltier heater (SM-4600, Scientifica, UK) and
576 temperature controller (Linlab2, Scientifica, UK), with a high-accuracy, low-noise temperature
577 control system, containing both a built-in temperature sensor and bath sensor for accurate
578 feedback. ACSF flow rates of ~3 ml/min were used to facilitate efficient heating/cooling.

579

580 To determine the effect of temperature on an activated cortical network, layer 4-evoked spiking
581 was quantified during perfusate temperature increases from 30°C to 36°C, and then to fever
582 range (~39°C) while recording membrane potential. The slicing plane facilitated clear
583 identification of whisker barrel columns, and neuronal activity was evoked by stimulating the
584 barrel center using a bipolar electrode (0.2 ms pulses) at a stimulation of 1.4 Eθ. Eθ is defined
585 as the minimal intensity that evoked a consistent excitatory postsynaptic current (EPSC) during
586 more than 3 of 5 consecutive sweeps with 10 s ISI (Antoine et al., 2019). Eθ was determined in
587 voltage clamp for each recorded cell prior to recording PSPs and spiking in current clamp. A
588 new brain slice was used for each recording. L4- evoked feedforward post synaptic potentials

589 (PSPs) and spiking were recorded in single L2/3 PNs from a pre-stimulus baseline membrane
590 potential (V_m) of -50 mV. This V_m, just below spike threshold, was selected to mimic *in vivo*
591 conditions, as PNs *in vivo* can reside within this V_m range during whisker exploration of objects
592 or surfaces (Yamashita et al., 2013). Evoked spikes were analyzed over a 150-ms interval,
593 starting 2-3 ms post-stimulus, for 11 sweeps at 10 s inter-sweep interval (ISI). Spike threshold
594 was defined as the membrane potential (V_m) at which the second derivative of V_m was >5 SDs
595 above the pre-stimulus period. Intrinsic spiking excitability was measured in the presence of
596 glutamate and GABA-A receptor blockers (in μM: 100 APV, 10 NBQX, 3 gabazine). F-I curves
597 were obtained from PNs held at –80 mV by applying incremental current injections relative to
598 this V_m.
599
600 **Animal Surgery and *In vivo* Electrophysiological Recordings**
601 *In vivo* experiments were done under general anesthesia where five mice (age, P24-26; body
602 weight, 7-10 g; both genders) received an intraperitoneal injection of ketamine (100 mg/kg) and
603 xylazine (10 mg/kg). Regular doses of the ketamine/xylazine cocktail were given intramuscularly
604 to maintain the depth of anesthesia during the experimental sessions. Up until the thermal fever
605 protocol started, the T_b of the animals was kept at 36°C using a homeothermic heating pad
606 connected to a temperature controller (Supertech, Pécs, Hungary). To measure the internal
607 body temperature, a Type T thermocouple microprobe (MT-29/5; Physitemp Instruments,
608 Clifton, NJ, USA) was placed in the rectum of the animal. The microprobe has a shaft diameter
609 of 330 μm, a time constant of 0.025 second and 0.1°C accuracy.
610
611 To perform high-density extracellular electrophysiological recordings, mice were placed in a
612 stereotaxic frame (David Kopf Instruments, Tujunga, CA, USA), then two circular craniotomies
613 (~1.5 mm in diameter) were made with a dental drill above the left and right barrel cortices. The

614 craniotomies were centered at the following stereotaxic coordinates: anterior-posterior (AP):
615 −1.0 mm; medial-lateral (ML): 3.5 mm (with respect to the bregma; Paxinos and Franklin 2001).
616 Two commercially available Neuropixels 1.0 silicon probes (imec, Leuven, Belgium; Jun et al.,
617 2017) mounted on two motorized stereotaxic micromanipulators (Neurostar, Tubingen,
618 Germany) were implanted into the brain, one into the left and the other into the right barrel
619 cortex, to a depth of 1.5 mm. An insertion speed of 2 μm/s was used to decrease the
620 mechanical trauma caused by the probe insertion (Fiáth et al. 2019).
621
622 In order for the probe tracks to be perpendicular to cortical layers, the probes were inserted at
623 an angle of 20 degrees from vertical. The dura mater in the craniotomy was left intact, except
624 when it was too thick and thus the silicon probe could not pierce through this layer (which was
625 indicated by significant probe buckling; n = 3 insertions). In these cases a 36 gauge, slightly
626 bent needle was used to carefully cut the dura above the targeted cortical area. After the probe
627 reached its final insertion depth, to allow the brain tissue to settle, we waited at least 10 minutes
628 before electrophysiological recording was started. Spiking activity of cortical neurons (action
629 potential band, 300–10.000 Hz) was recorded on 384 channels (768 channels in total for the
630 two probes), with a sampling rate of 30 kHz/channel and with a gain of 500 (yielding a resolution
631 of 2.34 μV per bit). Data were acquired using the SpikeGLX open-source software
632 (http://billkarsh.github.io/SpikeGLX/). A common stainless steel wire inserted into the neck
633 muscle of the animal served as the external reference and ground electrode. To avoid the
634 dehydration of the cortex, the skull and the craniotomy was kept moist during the whole
635 experiment using body temperature, sterile physiological saline solution and Gelaspon. Before
636 starting the experimental protocol, manual whisker stimulation (by repetitively touching the
637 whiskers of the animal with a cotton swab) was used to verify the recording position. In all cases
638 (n = 10 probe insertions), we detected strong whisker-evoked neuronal activity.
639

Thermal Fever Protocol during Electrophysiological Recordings

First, we recorded cortical activity for 45 minutes at ~36°C body temperature ("baseline " period), then the body temperature of the animal was elevated with the aid of the heating pad and a power bank with warming capability which was placed next to the mouse. The body temperature was increased from 36°C to 39°C in about 5 minutes (~0.01°C/s). The elevated body temperature was maintained for 45 minutes ("thermal fever " period). Next, we turned off the heating until the T_b reached physiological temperatures (36°C; ~5 min; ~0.01°C/s). Cortical activity was recorded for another 45 minutes at 36°C body temperature ("recovery " period). Continuous recordings with a total duration of 145 minutes were obtained for each mouse.

Spike Sorting and Data Analysis

To extract cortical single-unit activity, spike sorting was performed with Kilosort2 (https://github.com/MouseLand/Kilosort; Pachitariu et al., 2016a, 2016b) using the default parameter set (available in the StandardConfig.m file). Channels containing activity acquired by recording sites located outside the cortex were removed before spike sorting (usually ~130 channels/probe recorded from the barrel cortex). The list of single unit clusters generated by Kilosort2 was visually inspected to remove units considered as noise (e.g., units with abnormal spike waveform shapes) or multi-unit activity (e.g., clusters with a contaminated refractory period). Manual curation of the Kilosort2 results was done with the Phy Python library, which provides a graphical user interface for interactive visualization of high-density data and supply operations for merging, splitting and marking of clusters (https://github.com/cortex-lab/phy; Rossant et al., 2016). In this dataset, we aimed to keep only those single units which had at least 900 spikes (>~0.1 Hz firing rate), a clear refractory period, a consistent waveform shape and whose spikes were present throughout the 145-minute-long recording.

665 Following manual curation, based on their spike waveform duration, the selected single units (n
666 = 633) were separated into putative inhibitory interneurons and excitatory principal cells (Barthó
667 et al., 2004). The spike duration was calculated as the time difference between the trough and
668 the subsequent waveform peak of the mean filtered (300 – 6000 Hz bandpassed) spike
669 waveform. Durations of extracellularly recorded spikes showed a bimodal distribution
670 (Hartigan's dip test; $p < 0.001$) characteristic of the neocortex with shorter durations
671 corresponding to putative interneurons (narrow spikes) and longer durations to putative principal
672 cells (wide spikes). Next, k-means clustering was used to separate the single units into these
673 two groups, which resulted in 140 interneurons (spike duration < 0.6 ms) and 493 principal cells
674 (spike duration > 0.6 ms), corresponding to a typical 22% - 78% (interneuron – principal) cell
675 ratio. Finally, the firing rates of neurons were computed separately during the three
676 distinguished periods (baseline, thermal fever and recovery). To decrease the effect of transient
677 changes (e.g., tissue recovery during the baseline period or the short-term effect of heating
678 during the thermal fever period), for each 45-minute-long period, we used only the last 25-
679 minutes to calculate the mean firing rates of neurons.

680 **Immunofluorescence staining**
681

682 Mice were anesthetized and transcardially perfused using standard methods. Brains were post-
683 fixed overnight in 4% PFA at 4 °C with shaking, rinsed in 1X PBS, and cryoprotected in 30%
684 sucrose. They were embedded in optimal cutting temperature (OCT) compound, frozen on dry
685 ice, and stored at –80 °C until sectioning. Tissue was cut at 30 µm on a cryostat, mounted onto
686 slides. Sections were permeabilized in 0.3% Triton X-100 (in 1X PBS) for 10 min at room
687 temperature. Endogenous peroxidase activity was quenched by incubation in 3% H_2O_2 (in 1X
688 PBS) at room temperature. Slides were blocked in 10% normal goat serum for 1 h at room
689 temperature, then incubated overnight at 4 °C with anti-TRPV3-Biotin antibody (#ACC-033-B),
690 TRPV3 blocking peptide (#BLP-CC033), and/or anti-TRPV4 antibody(#ACC-034) (Alomone

691 Labs, Israel). For antibody–peptide controls, the anti-TRPV3-Biotin antibody was pre-incubated
692 with its blocking peptide at a 1:2.5 ratio, using 1 mg/ml of each. The following day, sections
693 were incubated for 1 h at room temperature with fluorescently labeled secondary antibodies
694 (streptavidin-conjugated or unconjugated). Nuclei were counterstained with DAPI Fluoromount-
695 G (Electron Microscopy Sciences, USA). Finally, sections were mounted onto slides, cover-
696 slipped, and stored at 4 °C until imaging. Images were acquired using a Keyence BZ-X810
697 microscope (BZ-X800 Viewer, Version 1.1.1.8) with BZ-X filter sets: DAPI (Ex 360/40 nm; OP-
698 87762), GFP (Ex 470/40 nm; OP-87763), and TRITC (Ex 545/25 nm; OP-87764).

699
700 **Statistics**

701 Statistical analyses were conducted using Prism 9.0 (GraphPad). For experiments, at least 3
702 mice from a minimum of 2 separate litters were used, with littermates typically included across
703 the age groups P7-8, P12-14, and P20-23. Non-Gaussian data were either log-transformed for
704 parametric testing or subjected to nonparametric tests, as specified in the results and figure
705 legends. Significance was consistently reported at $\alpha = 0.05$. Details on the statistical tests used
706 are provided in the figure captions.

707
708 **References**
709

710 Antoine, M. W., T. Langberg, P. Schnepel, and D. E. Feldman.(2019) Increased Excitation-
711 Inhibition Ratio Stabilizes Synapse and Circuit Excitability in Four Autism Mouse Models.
712 *Neuron* 101, no. 4: 648-61 e4. https://doi.org/10.1016/j.neuron.2018.12.026.
713 Baram, T. Z., A. Gerth, and L. Schultz.(1997) Febrile Seizures: An Appropriate-Aged Model
714 Suitable for Long-Term Studies. *Brain Res Dev Brain Res* 98, no. 2: 265-70.
715 https://doi.org/10.1016/s0165-3806(96)00190-3.
716 Bartho, P., H. Hirase, L. Monconduit, M. Zugaro, K. D. Harris, and G. Buzsaki.(2004)
717 Characterization of Neocortical Principal Cells and Interneurons by Network Interactions
718 and Extracellular Features. *J Neurophysiol* 92, no. 1: 600-8.
719 https://doi.org/10.1152/jn.01170.2003.
720 Bender, R. A., C. Dubé, and T. Z. Baram. (2004). Febrile seizures and mechanisms of
721 epileptogenesis: insights from an animal model. *Adv Exp Med Biol* 548: 213–225.
722 https://doi.org/10.1007/978-1-4757-6376-8_15
723 Bhatia, A., S. Moza, and U. S. Bhalla.(2019) Precise Excitation-Inhibition Balance Controls Gain
724 and Timing in the Hippocampus. *Elife* 8. https://doi.org/10.7554/eLife.43415.

725 Campbell, I.(2011) Body Temperature and Its Regulation. *Anaesthesia and Intensive Care*
726 *Medicine* 12, no. 6: 240-44. https://doi.org/DOI 10.1016/j.mpaic.2011.03.002.
727 Caterina, M. J.(2007) Transient Receptor Potential Ion Channels as Participants in
728 Thermosensation and Thermoregulation. *Am J Physiol Regul Integr Comp Physiol* 292,
729 no. 1: R64-76. https://doi.org/10.1152/ajpregu.00446.2006.
730 Chen, X., J. Zhang, and K. Wang.(2022) Inhibition of Intracellular Proton-Sensitive Ca(2+)-
731 Permeable Trpv3 Channels Protects against Ischemic Brain Injury. *Acta Pharm Sin B*
732 12, no. 5: 2330-47. https://doi.org/10.1016/j.apsb.2022.01.001.
733 Dobbing, J., and J. Sands. (1973). Quantitative growth and development of human brain. *Arch*
734 *Dis Child* 48: 757–767. https://doi.org/10.1136/adc.48.10.757
735 Dube, C. M., T. Ravizza, M. Hamamura, Q. Zha, A. Keebaugh, K. Fok, A. L. Andres*, et*
736 *al.*(2010) Epileptogenesis Provoked by Prolonged Experimental Febrile Seizures:
737 Mechanisms and Biomarkers. *J Neurosci* 30, no. 22: 7484-94.
738 https://doi.org/10.1523/JNEUROSCI.0551-10.2010.
739 Fiath, R., A. L. Marton, F. Matyas, D. Pinke, G. Marton, K. Toth, and I. Ulbert.(2019) Slow
740 Insertion of Silicon Probes Improves the Quality of Acute Neuronal Recordings. *Sci Rep*
741 9, no. 1: 111. https://doi.org/10.1038/s41598-018-36816-z.
742 Hankenson, F. C., J. O. Marx, C. J. Gordon, and J. M. David.(2018) Effects of Rodent
743 Thermoregulation on Animal Models in the Research Environment. *Comp Med* 68, no. 6:
744 425-38. https://doi.org/10.30802/AALAS-CM-18-000049.
745 Hardingham, N. R., and A. U. Larkman.(1998) Rapid Report: The Reliability of Excitatory
746 Synaptic Transmission in Slices of Rat Visual Cortex in Vitro Is Temperature Dependent.
747 *J Physiol* 507 (Pt 1), no. Pt 1: 249-56. https://doi.org/10.1111/j.1469-
748 7793.1998.249bu.x.
749 Holtzman, D., K. Obana, and J. Olson.(1981) Hyperthermia-Induced Seizures in the Rat Pup: A
750 Model for Febrile Convulsions in Children. *Science* 213, no. 4511: 1034-6.
751 https://doi.org/10.1126/science.7268407.
752 Jun, J. J., N. A. Steinmetz, J. H. Siegle, D. J. Denman, M. Bauza, B. Barbarits, A. K. Lee*, et*
753 *al.*(2017) Fully Integrated Silicon Probes for High-Density Recording of Neural Activity.
754 *Nature* 551, no. 7679: 232-36. https://doi.org/10.1038/nature24636.
755 Kanju, P., and W. Liedtke.(2016) Pleiotropic Function of Trpv4 Ion Channels in the Central
756 Nervous System. *Exp Physiol* 101, no. 12: 1472-76. https://doi.org/10.1113/EP085790.
757 Kashio, M., and M. Tominaga.(2022) Trp Channels in Thermosensation. *Curr Opin Neurobiol*
758 75: 102591. https://doi.org/10.1016/j.conb.2022.102591.
759 Kim, J. A., and B. W. Connors.(2012) High Temperatures Alter Physiological Properties of
760 Pyramidal Cells and Inhibitory Interneurons in Hippocampus. *Front Cell Neurosci* 6: 27.
761 https://doi.org/10.3389/fncel.2012.00027.
762 Kiyatkin, E. A.(2019) Brain Temperature and Its Role in Physiology and Pathophysiology:
763 Lessons from 20 Years of Thermorecording. *Temperature (Austin)* 6, no. 4: 271-333.
764 https://doi.org/10.1080/23328940.2019.1691896.
765 Lee, J., J. Urban-Ciecko, E. Park, M. Zhu, S. E. Myal, D. J. Margolis, and A. L. Barth.(2021)
766 Fosgfp Expression Does Not Capture a Sensory Learning-Related Engram in Superficial
767 Layers of Mouse Barrel Cortex. *Proc Natl Acad Sci U S A* 118, no. 52.
768 https://doi.org/10.1073/pnas.2112212118.
769 Miller, D. J., and P. E. Fort.(2018) Heat Shock Proteins Regulatory Role in Neurodevelopment.
770 *Front Neurosci* 12: 821. https://doi.org/10.3389/fnins.2018.00821.
771 Moqrich A., S. W. Hwang, T. J. Earley, M. J. Petrus, A. N. Murray, K. S. Spencer, M. Andahazy,
772 G. M. Story, and A. Patapoutian.(2005) Impaired Thermosensation in Mice Lacking
773 Trpv3, a Heat and Camphor Sensor in the Skin. *Science* 307, no. 5714: 1468-72.
774 https://doi.org/10.1126/science.1108609.

Moussaieff, A., N. Rimmerman, T. Bregman, A. Straiker, C. C. Felder, S. Shoham, Y. Kashman, *et al.*(2008) Incensole Acetate, an Incense Component, Elicits Psychoactivity by Activating Trpv3 Channels in the Brain. *FASEB J* 22, no. 8: 3024-34. https://doi.org/10.1096/fj.07-101865.

Oakley, J. C., F. Kalume, F. H. Yu, T. Scheuer, and W. A. Catterall.(2009) Temperature- and Age-Dependent Seizures in a Mouse Model of Severe Myoclonic Epilepsy in Infancy. *Proc Natl Acad Sci U S A* 106, no. 10: 3994-9. https://doi.org/10.1073/pnas.0813330106.

Pachitariu, M., N. Steinmetz, S. Kadir, M. Carandini, and K. Harris.(2016) Fast and Accurate Spike Sorting of High-Channel Count Probes with Kilosort. *Advances in Neural Information Processing Systems 29 (Nips 2016)* 29.

Pachitariu, Marius, Nicholas A. Steinmetz, Shabnam N. Kadir, Matteo Carandini, and Harris %J bioRxiv Kenneth D.(2016) Kilosort: Realtime Spike-Sorting for Extracellular Electrophysiology with Hundreds of Channels.

Paxinos G, Franklin KBJ. (2001)The Mouse Brain in Stereotaxic Coordinates. Academic Press, London, UK: Elsevier Science, 2001.

Rossant, C., S. N. Kadir, D. F. M. Goodman, J. Schulman, M. L. D. Hunter, A. B. Saleem, A. Grosmark, *et al.*(2016) Spike Sorting for Large, Dense Electrode Arrays. *Nat Neurosci* 19, no. 4: 634-41. https://doi.org/10.1038/nn.4268.

Shibasaki, K., M. Suzuki, A. Mizuno, and M. Tominaga.(2007) Effects of Body Temperature on Neural Activity in the Hippocampus: Regulation of Resting Membrane Potentials by Transient Receptor Potential Vanilloid 4. *J Neurosci* 27, no. 7: 1566-75. https://doi.org/10.1523/JNEUROSCI.4284-06.2007.

Shinnar, S., and C. O'Dell.(2004) Febrile Seizures. *Pediatr Ann* 33, no. 6: 394-401. https://doi.org/10.3928/0090-4481-20040601-10.

Smith, G. D., M. J. Gunthorpe, R. E. Kelsell, P. D. Hayes, P. Reilly, P. Facer, J. E. Wright, *et al.*(2002) Trpv3 Is a Temperature-Sensitive Vanilloid Receptor-Like Protein. *Nature* 418, no. 6894: 186-90. https://doi.org/10.1038/nature00894.

Su, W., X. Qiao, W. Wang, S. He, K. Liang, and X. Hong.(2023) Trpv3: Structure, Diseases and Modulators. *Molecules* 28, no. 2. https://doi.org/10.3390/molecules28020774.

Vincent, F., A. Acevedo, M. T. Nguyen, M. Dourado, J. DeFalco, A. Gustafson, P. Spiro, *et al.*(2009) Identification and Characterization of Novel Trpv4 Modulators. *Biochem Biophys Res Commun* 389, no. 3: 490-4. https://doi.org/10.1016/j.bbrc.2009.09.007.

Wang, H., B. Wang, K. P. Normoyle, K. Jackson, K. Spitler, M. F. Sharrock, C. M. Miller, *et al.*(2014) Brain Temperature and Its Fundamental Properties: A Review for Clinical Neuroscientists. *Front Neurosci* 8: 307. https://doi.org/10.3389/fnins.2014.00307.

Xu, H., I. S. Ramsey, S. A. Kotecha, M. M. Moran, J. A. Chong, D. Lawson, P. Ge, *et al.*(2002) Trpv3 Is a Calcium-Permeable Temperature-Sensitive Cation Channel. *Nature* 418, no. 6894: 181-6. https://doi.org/10.1038/nature00882.

Yamashita, T., A. Pala, L. Pedrido, Y. Kremer, E. Welker, and C. C. Petersen.(2013) Membrane Potential Dynamics of Neocortical Projection Neurons Driving Target-Specific Signals. *Neuron* 80, no. 6: 1477-90. https://doi.org/10.1016/j.neuron.2013.10.059.

Zhang, H., X. Sun, H. Qi, Q. Ma, Q. Zhou, W. Wang, and K. Wang.(2019) Pharmacological Inhibition of the Temperature-Sensitive and Ca(2+)-Permeable Transient Receptor Potential Vanilloid Trpv3 Channel by Natural Forsythoside B Attenuates Pruritus and Cytotoxicity of Keratinocytes. *J Pharmacol Exp Ther* 368, no. 1: 21-31. https://doi.org/10.1124/jpet.118.254045.

Figures and Figure Legends

824 **Figure 1: Body Temperature rises to fever levels during regular activity and upon**
825 **exposure to higher ambient temperatures.**
826 **A.** Left: Setup for recording mouse body temperature (T_b) at room temperature using an
827 implanted transponder for non-invasive measurement. Right: Average T_b readings over 6 hours
828 at 5-minute intervals for 10 mice. T_b typically hovers around 36.5°C during the day.
829 **B.** T_b may briefly elevate into fever range (shaded red bars) during regular daily activity. Median
830 with upper and lower limits indicated.
831 **C.** T_b readings over 6 hours, at 5-minute intervals for animal 3 in Figure 1B. Shaded red dots
832 indicate time points when T_b enters the fever range.
833 **D.** Left: Setup for T_b recordings during infrared light exposure. Right: T_b elevates into the fever
834 range (>38°C) for extended durations, lasting minutes to hours. Average T_b readings over 6
835 hours at 5-minute intervals for 10 mice.

836 **Figure 2: Spiking in P12-14 cortical excitatory pyramidal neurons remains stable as**
837 **temperature enters the fever range.**
838 **A.** Setup for recording L4-evoked postsynaptic potential and spiking in a cortical excitatory
839 pyramidal neuron (PN) at just-subthreshold V_m at 30°C, 36°C and 39°C in mouse primary
840 somatosensory (S1) cortex.
841 **B.** Example traces of L4-evoked spikes in L2/3 PN during consecutive recordings at 30°C
842 (black), 36°C (gray), and 39°C (red).
843 **C.** Depolarization required to reach spike threshold (ST) in L2/3 PNs during temperature
844 elevations from 30°C to 39°C.
845 **D.** Same as (C) for input resistance (R_{in}).
846 **E.** Same as (C) for the percentage of spiking L2/3 PNs.
847 **F.** Same as in (C) for the spiking distribution.
848 **G.** Same as in (C) for the number of spikes.
849 **H.** Rheobase in L2/3 PNs during temperature elevations from 30°C to 39°C. 8 PNs recorded
850 from 3 animals.
851 **I.** Quantification of evoked spiking for F-I curves in L2/3 PNs during temperature elevations from
852 30°C to 39°C. Each recorded cell was exposed to the full temperature range (30 to 39°C). 8
853 PNs recorded from 3 animals.
854 In **C**, **D** and **G**, each data point represents an individual cell. In C-F, 37 PNs recorded from 14
855 animals, with each cell exposed to temperature elevations from 30°C to 39°C. Data in **C**, **D**, and
856 **G** are shown as mean ± SEM. Statistical significance was assessed as follows: **C**, **D**, **G** :one-
857 way repeated-measures ANOVA with Tukey's post-hoc test ($\alpha = 0.05$); E – two-tailed binomial

858 test; F – Kolmogorov–Smirnov (K–S) test, **H**: two-way repeated-measures ANOVA with Tukey's
859 post-hoc test(α = 0.05).

860

861 **Figure 3: Spiking in P7-8 cortical excitatory pyramidal neurons decreases as temperature**
862 **enters the fever range.**

863 **A.** Setup for recording L4-evoked postsynaptic potential and spiking in an excitatory pyramidal
864 neuron (PN) at just-subthreshold V_m at 30°C, 36°C and 39°C in mouse primary somatosensory
865 (S1) cortex.
866 **B.** Example traces of L4-evoked spikes in L2/3 PN during consecutive recordings at 30°C
867 (black), 36°C (gray), and 39°C (red).
868 **C.** Depolarization required to reach spike threshold (ST) in L2/3 PNs during temperature
869 elevations from 30°C to 39°C.
870 **D.** Same as (C) for input resistance (R_{in}).
871 **E.** Same as (C) for the percentage of spiking L2/3 PNs.
872 **F.** Same as in (C) for the spiking distribution.
873 **G.** Same as in (C) for the number of spikes.
874 In **C**, **D** and **G**, each data point represents an individual cell. In C-G, 19 PNs recorded from 5
875 animals, with each cell exposed to temperature elevations from 30°C to 39°C. Data in **C**, **D**, and
876 **G** are shown as mean ± SEM. Statistical significance was assessed as follows: **C**, **D**, **G** :one-
877 way repeated-measures ANOVA with Tukey's post-hoc test (α = 0.05); E – two-tailed binomial
878 test; F – Kolmogorov–Smirnov test.

879 **Figure 4: Increased depolarization at higher spike thresholds helps maintain stable**
880 **spiking activity in cortical pyramidal neurons during temperature elevations.**
881 **A.** Illustration demonstrating how temperature-induced changes in spike threshold make spiking
882 more challenging for a neuron, requiring larger levels of depolarization to sustain spiking.
883 **B.** Example traces of L4-evoked postsynaptic potentials (PSPs) in L2/3 PN during consecutive
884 recordings at 30°C (black), 36°C (gray), and 39°C (red).
885 **C**. Correlation of PSP peak versus spike threshold (ST). r = Pearson correlation coefficient with
886 Deming linear regression.
887 **D.** Correlation of input resistance versus ST. r = Pearson correlation coefficient with
888 simple linear regression.
889 **E.** Same as D but for input resistance versus PSP.

890 **F.** Illustration showing how temperature-induced loss in inhibition (blue IPSP) could lead to
891 larger levels of depolarization. IPSPs typically bring the membrane potential away from the
892 spike threshold.
893 **G.** The late PSP peak in L2/3 PNs during temperature elevations from 30°C to 39°C.
894 Statistical significance was evaluated on log-transformed data using one-way repeated
895 measures ANOVA with Tukey's test, with significance at α=0.05.
896 **H**. Same as D but for PSP versus Late PSP Peak. r = Spearman correlation coefficient with
897 simple linear regression.
898
899 **Figure 5: Cortical excitatory neurons that remain active at febrile temperatures exhibit**
900 **increased spiking rates.**
901 **A.** Setup for *in vivo* recording of spiking in mouse S1 cortex during temperature increases from
902 36°C to 39°C and cooling back to 36°C.
903 **B.** Color maps (with yellow and red indicating spiking activity) illustrate multiunit activity obtained
904 in the left and right cortices during baseline temperature (left), warming to fever T_b (middle), and
905 cooling back to 36°C (recovery upon heat removal).
906 **C.** Example traces of spiking activity recorded from three cortical positions (marked by black,
907 gray, and white asterisks on the right side of panels in figure 5B.
908 **D.** Mean spike waveforms (black), single spikes (gray) and autocorrelograms (bottom) of single
909 units isolated, with unit 3 representing a putative interneuron.
910 **E.** Normalized firing rates of putative excitatory PNs and interneurons obtained from recordings
911 in A.
912 **F.** The normalized firing rates of five representative units during the baseline, warming (red
913 shaded area), and recovery periods. Figure 5F presents the same data, with color coding
914 consistent with the units in Figure 5D.
915 **G.** Left: Setup for *ex vivo* recording of L4-evoked postsynaptic potentials and spiking in L2/3
916 cortical PN at just-subthreshold V_m at 30°C, 36°C and 39°C in mouse S1 cortex.
917 Right: Percent distribution for recorded PNs that never spiked, stopped spiking, stayed spiking,
918 or started spiking during temperature increases from 36°C to 39°C.
919 **H.** L2/3 PN spiking activity in neurons that stayed spiking (left), started spiking (middle), and
920 stopped spiking (right) upon temperature increases from 36°C to 39°C.
921 **I.** Activity distribution for *ex vivo* recorded neurons that never spiked, and those that stopped
922 spiking, stayed spiking, or started spiking upon temperature increases from 36°C to 39°C. P-
923 value = 0.01 indicates a significant increase in the fraction of neurons that stayed spiking during
924 temperature increases from 36°C to 39°C (solid red bar).

925 In **E** and **H**, each data point represents an individual animal and cell, respectively. Data were
926 collected from 5 animals in **B–F**, 11 animals in **G–H**, and 9–14 animals in **I**. Statistical
927 significance was assessed using one-way repeated-measures ANOVA with Tukey's post-hoc
928 test (**E**), paired two-tailed t-test (**H**), and binomial test (**I**), with significance set at α = 0.05.
929
930 **Figure 6: Excitatory pyramidal neurons that remain spiking with temperature elevations**
931 **into fever range exhibit unique intrinsic properties.**
932 Neurons that spiked at all temperatures (30°C, 36°C, and 39°C) are STAY PNs, while those that
933 stopped spiking at 36°C or 39°C are STOP neurons.
934 **A.** Depolarization required to reach spike threshold (ST) in STOP and STAY L2/3 PNs during
935 temperature elevations from 30°C to 39°C.
936 **B.** Same as (A) for L4-evoked postsynaptic potentials (PSPs)
937 **C.** Correlation of PSP peak versus ST in STAY L2/3 PNs at 30°C, 36°C, and 39°C. r = Pearson
938 correlation coefficient with Deming linear regression.
939 **D.** Same as (C) for STOP cells.
940 **E.** Same as (A) for the L4-evoked late PSP peak.
941 **F.** Same as (A) for spike height.
942 **G.** Same as (A) for spike afterhyperpolarization (AHP).
943 **H.** Same as (A) for input resistance.
944 Each data point in **A–H** represents an individual cell. Data were collected from 14 animals.
945 Mean ± SEM is shown in **A–B** and **E–H**. Statistical significance was assessed using one- or
946 two-way repeated-measures ANOVA with Tukey's or Sidak post-hoc test (**A–B**, **E–H**; α = 0.05).
947 In **C–D**, correlations were evaluated using Pearson's r with Deming linear regression.
948

949 **Figure 7. TRPV3 protein expression by immunohistochemistry at postnatal days 7, 14,**
950 **and 21.**
951 **A.** TRPV3 immunostaining (green) in mouse primary somatosensory (S1) cortex, striatum,
952 thalamus, and hippocampus, with DAPI counterstain (blue).
953 Top row left: Postnatal day (P)7; bottom row left: P14; bottom row right: P21.
954 Top row right: Sections incubated with TRPV3 antibody plus TRPV3 blocking peptide in S1
955 cortex, striatum, thalamus, and hippocampus (green) with DAPI counterstain (blue). Remaining
956 TRPV3 staining is shown in green with DAPI in blue.
957 **B.** TRPV3 and TRPV4 immunostaining in S1 cortex, striatum, thalamus, and hippocampus at
958 P14.
959 Top row left: TRPV3 (green) and TRPV4 (brick red).

960 Top row right: TRPV3 (green) and TRPV4 (brick red) with DAPI counterstain (blue).
961 Bottom row left: TRPV4 immunostaining in S1BF (inset from top row left) at 10×.
962 Bottom row right: TRPV3 immunostaining in S1BF (inset from top row left) at 10×.

963 **Figure 8: Temperature elevations in fever range increase TRPV3 currents in cortical**
964 **pyramidal neurons.**
965 **A.** Setup for recording whole-cell TRPV3 currents at 30°C (black), 36 °C (grey) and 39°C (red).
966 in cortical excitatory pyramidal neurons (PNs) with bath application of camphor (5mM), a *TPRV3*
967 agonist.
968 **B.** Current density-voltage (I-V) relationship of TRPV3 currents at 30°C (black), 36 °C (grey) and
969 39°C (red) in WT mice: 11 cells from 4 mice.
970 **C.** Scatter dot plots of the current density-voltage measurements.
971 **D.** Current density-voltage (I-V) relationship of TRPV3 currents at 30°C (black) in the presence
972 of camphor (5mM), a TPRV3 agonist, or camphor (5mM) + TRPV3 blocker (Forsythoside B, 50
973 μM) (blue).
974 **E.** Same as (**D**) but for 36°C.
975 **F.** Same as (**D**) but for 39°C.
976 **G.** Current density-voltage (I-V) plot showing the net TRPV3 current (opener – (opener+
977 blocker) condition).
978 In B-F, statistical significance was assessed using a two-way repeated-measures ANOVA with
979 Tukey's or Sidak post-hoc test (α = 0.05)
980

981 **Figure 9: Inhibiting TRPV3, but not TRPV4 channels, significantly reduced the population**
982 **of STAY pyramidal neurons and spiking levels at fever temperature.**
983 **A.** Setup for recording L4-evoked postsynaptic potential and spiking in an excitatory cortical
984 pyramidal neuron (PN) with an intracellular blocker of TRPV3 channels (Forsythoside B, 50 μM)
985 (left) or TRPV4 channels (RN1734, 10 μM) (right) at just-subthreshold V_m at 30°C, 36°C, and
986 39°C in mouse S1 cortex.
987 **B.** Percentages of cell types obtained from experiment in A.
988 **C.** Evoked spikes in L2/3 cortical PNs during temperature elevations to 30°C, 36°C, and 39°C
989 under three conditions: no blockers, TRPV3 blocker (Forsythoside B, 50 μM), or TRPV4 blocker
990 (RN1734, 10 μM).
991 **D.** Correlation between PSP peak and spike threshold (ST). r = Pearson correlation coefficient
992 with Deming linear regression.
993 **E.** Same as (C) for the L4-evoked late PSP peak.
994 **F.** Same as (C) for input resistance (R_{in}).

995 Each data point in **C–F** represents an individual cell. Data were collected from 26 cells in 7
996 animals for the TRPV3 blocker, 24 cells in 6 animals for the TRPV4 blocker, and 37 cells in 14
997 animals for the no-block condition. Mean ± SEM is shown in **C, E, and F**. Statistical significance
998 was assessed using one- or two-way repeated-measures ANOVA with Tukey's or Sidak post-
999 hoc test (α = 0.05). In **D**, correlations were evaluated using Pearson's r with Deming linear
1000 regression.

1001 **Figure 10: TRPV3 knockout mice exhibit reduced spiking activity at febrile temperatures**
1002 **and delayed seizure onset.**
1003 **A.** Setup for recording L4-evoked postsynaptic potentials and spiking in excitatory cortical
1004 pyramidal neurons (PNs) at just-subthreshold Vm at 30 °C, 36 °C, and 39 °C in mouse S1
1005 cortex of wildtype (*Trpv3*$^{+/+}$) and Trpv3 knockout (*Trpv3*$^{-/-}$) mice.
1006 **B.** Depolarization required to reach spike threshold (ST) in *Trpv3*$^{+/+}$ and *Trpv3*$^{-/-}$ mice at 30°C,
1007 36°C, and 39°C.
1008 **C.** Same as (B) but for input resistance (R_{in}).
1009 **D.** Same as (B) but for number of spikes.
1010 **E.** Same as (B) but for postsynaptic potential (PSP).
1011 **F.** Setup for recording mouse body temperature (T_b) at room temperature and during fever-
1012 range and higher, using an implanted transponder for non-invasive measurement, with
1013 exposure to infrared light.
1014 **G.** Time to loss of postural control (LPC), defined as collapse and failure to maintain upright
1015 posture, in wildtype (*Trpv3*$^{+/+}$), heterozygous (*Trpv3*$^{+/-}$) and Trpv3 knockout (*Trpv3*$^{-/-}$) mice.
1016 **H.** Same as in (G) but showing T_b at seizure onset.
1017 **I.** Same as in (G) but for the time from LPC to seizure onset.
1018 Each data point in **B–E** represents an individual cell (3 animals per genotype). Statistical
1019 significance was assessed using two-way repeated-measures ANOVA with Tukey's or Sidak
1020 post-hoc test (α = 0.05). Each data point in **G–I** represents an individual animal. Statistical
1021 significance was assessed using one-way repeated-measures ANOVA with Tukey's or Sidak
1022 post-hoc test (α = 0.05).

1023 **Figure 11. Summary model of how STAY neurons achieve firing stability through unique**
1024 **ion channel compositions, including TRPV3.**
1025 **A.** In cortical L2/3 pyramidal neurons (PNs) with synaptically evoked spiking, gradual increases
1026 in brain slice temperature from 30 °C to 36 °C to 39 °C result in four possible outcomes:
1027 neurons remain inactive, continue spiking (STAY), stop spiking, or initiate spiking. To spike, PNs
1028 must reach spike threshold (ST), defined as the minimal V_m that elicits an action potential, which

1029 requires sufficient depolarization via the postsynaptic potential (PSP). STAY neurons
1030 consistently reach ST and continue spiking. Neurons that stop spiking fall below the level of
1031 depolarization required to reach ST, while neurons that initiate spiking achieve sufficient
1032 depolarization to newly reach ST.
1033 **B.** STAY neurons may contain unique ion channels, such as TRPV3. TRPV3 channels are
1034 highly permeable to Ca^{2+} ions, and Ca^{2+} influx contributes to PN depolarization. The presence of
1035 TRPV3 facilitates greater ion entry, enabling depolarization sufficient to reach ST and sustain
1036 spiking, whereas its absence reduces depolarization to levels insufficient for spiking.

1037

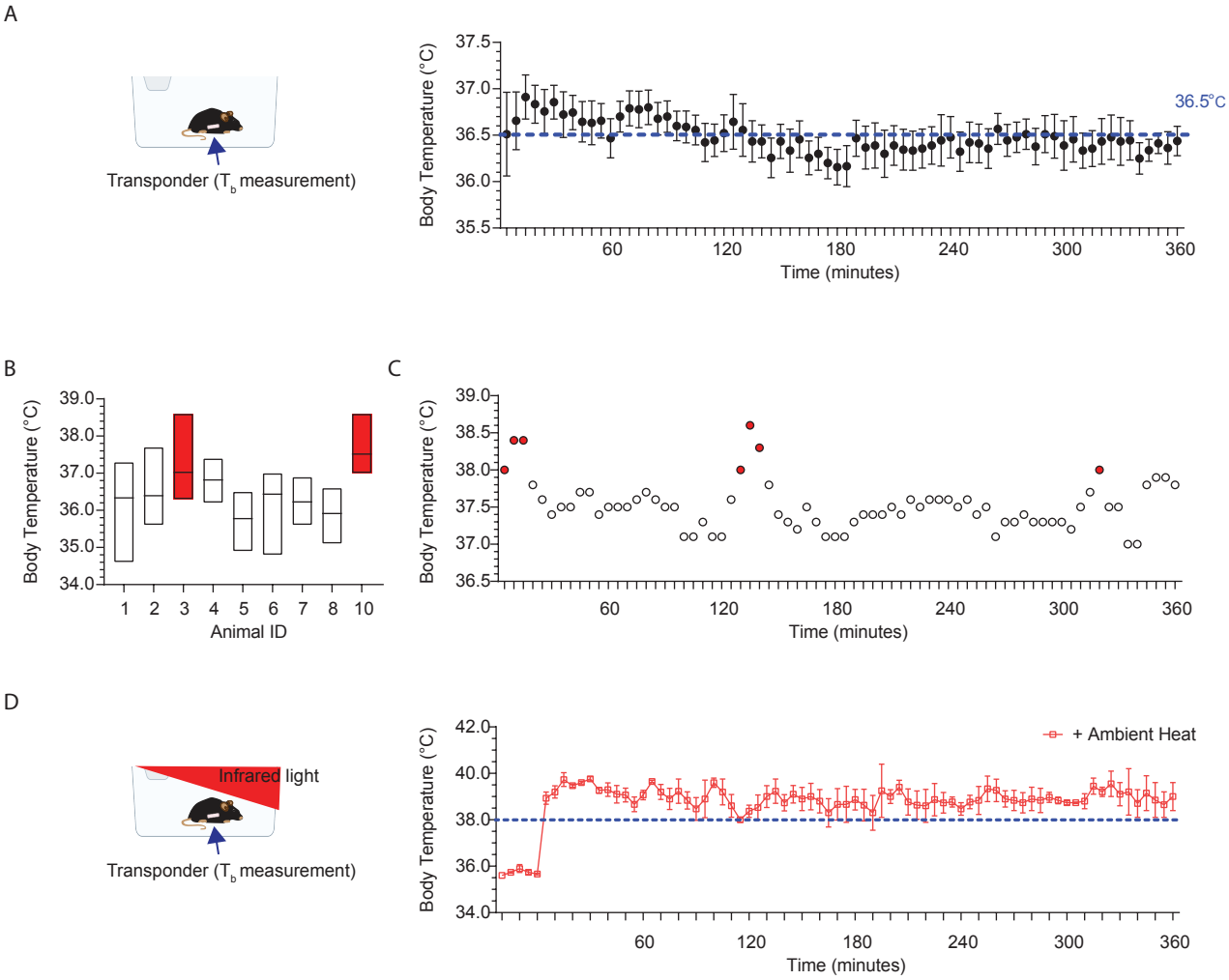

Figure 1: **Body Temperature rises to fever levels during regular activity and upon exposure to higher ambient temperatures.**
A. Left: Setup for recording mouse body temperature(T_b) at room temperature using an implanted transponder for non-invasive measurement. Right: Average T_b readings over 6 hours at 5-minute intervals for 10 mice. T_b typically hovers around 36.5°C during the day.
B. T_b may briefly elevate into fever range (shaded red bars) during regular daily activity. Median with upper and lower limits indicated.
C. T_b readings over 6 hours, at 5-minute intervals for animal 3 in Figure 1B. Shaded red dots indicate time points when T_b enters the fever range.
D. Left: Setup for T_b recordings during infrared light exposure. Right: T_b elevates into the fever range (>38°C) for extended durations, lasting minutes to hours. Average T_b readings over 6 hours at 5-minute intervals for 10 mice.

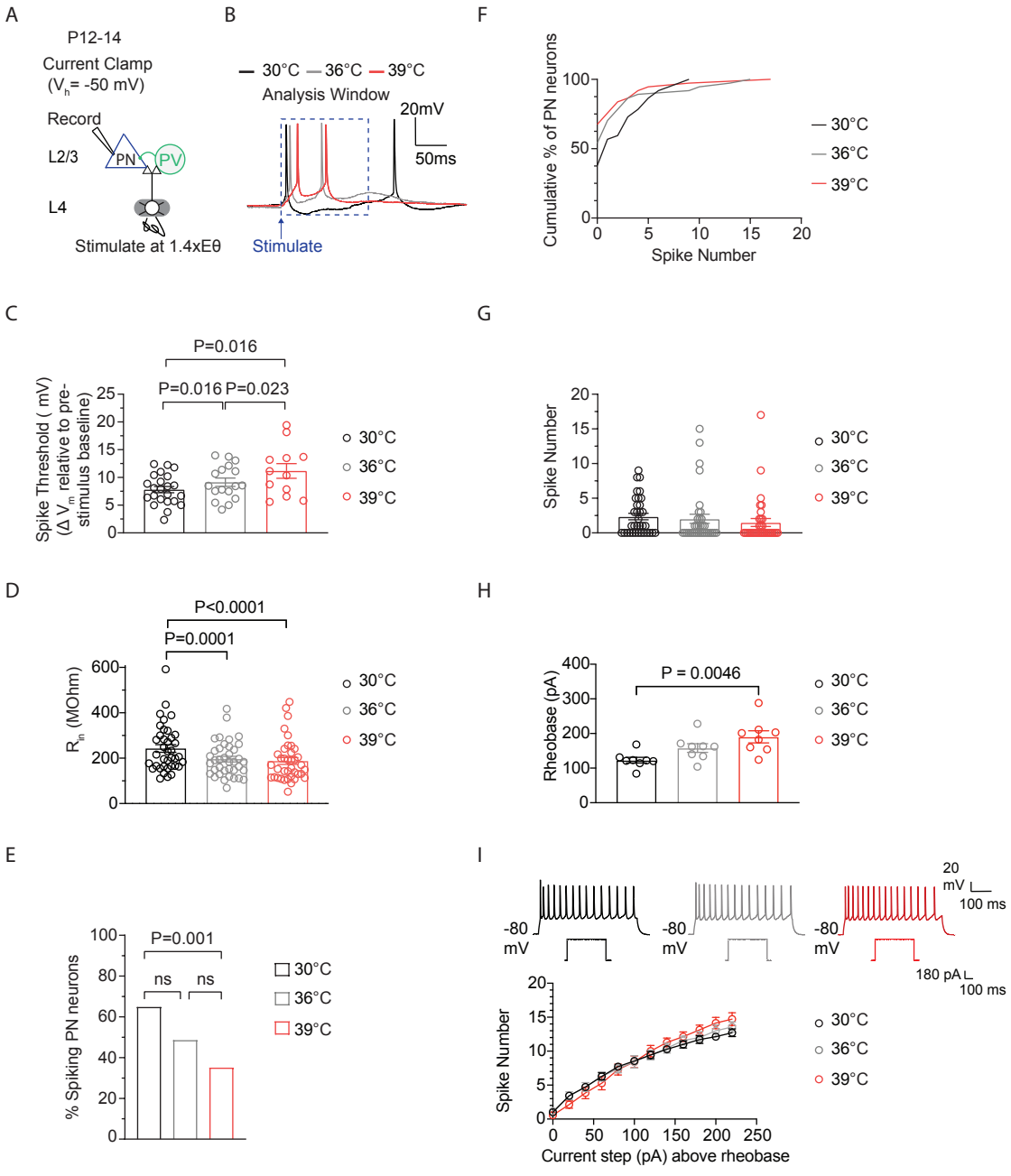

Figure 2: **Spiking in P12-14 cortical excitatory pyramidal neurons remains stable as temperature enters the fever range.**
A. Setup for recording L4-evoked postsynaptic potential and spiking in a cortical excitatory pyramidal neuron (PN) at just-subthreshold V_m at 30°C, 36°C and 39°C in mouse primary somatosensory (S1) cortex.
B. Example traces of L4-evoked spikes in L2/3 PN during consecutive recordings at 30°C (black), 36°C (gray), and 39°C (red).
C. Depolarization required to reach spike threshold (ST) in L2/3 PNs during temperature elevations from 30°C to 39°C.
D. Same as (C) for input resistance (R_{in}).
E. Same as (C) for the percentage of spiking L2/3 PNs.
F. Same as in (C) for the spiking distribution.
G. Same as in (C) for the number of spikes.
H. Rheobase in L2/3 PNs during temperature elevations from 30°C to 39°C. 8 PNs recorded from 2 animals.
I. Quantification of evoked spiking for F-I curves in L2/3 PNs during temperature elevations from 30°C to 39°C. Each recorded cell was exposed to the full temperature range (30 to 39°C). 8 PNs recorded from 3 animals.
In C, D and G, each data point represents an individual cell. In C-F, 37 PNs recorded from 14 animals, with each cell exposed to temperature elevations from 30°C to 39°C. Data in C, D, and G are shown as mean ± SEM. Statistical significance was assessed as follows: C, D, G :one-way repeated-measures ANOVA with Tukey's post-hoc test (α = 0.05); E – two-tailed binomial test; F – Kolmogorov–Smirnov (K–S) test, H: two-way repeated-measures ANOVA with Tukey's post-hoc test(α = 0.05).

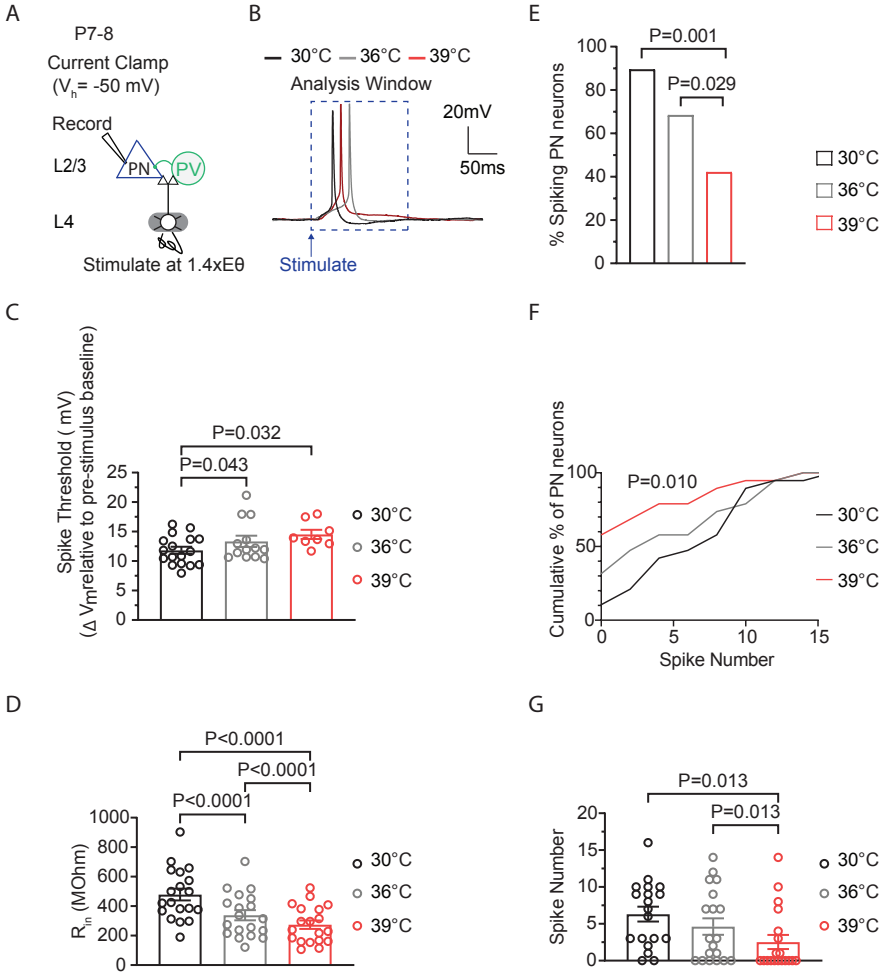

Figure 3: Spiking in P7-8 cortical pyramidal neurons decreases as temperature enters the fever range.
A. Setup for recording L4-evoked postsynaptic potential and spiking in an excitatory pyramidal neuron (PN) at just-subthreshold V_m at 30°C, 36°C and 39°C in mouse primary somatosensory (S1) cortex.
B. Example traces of L4-evoked spikes in L2/3 PN during consecutive recordings at 30°C (black), 36°C (gray), and 39°C (red).
C. Depolarization required to reach spike threshold (ST) in L2/3 PNs during temperature elevations from 30°C to 39°C.
D. Same as (C) for input resistance (R_{in}).
E. Same as (C) for the percentage of spiking L2/3 PNs.
F. Same as in (C) for the spiking distribution.
G. Same as in (C) for the number of spikes.
In C, D and G, each data point represents an individual cell. In C-G, 19 PNs recorded from 5 animals, with each cell exposed to temperature elevations from 30°C to 39°C. Data in C, D, and G are shown as mean ± SEM. Statistical significance was assessed as follows: C, D, G :one-way repeated-measures ANOVA with Tukey's post-hoc test (α = 0.05); E – two-tailed binomial test; F – Kolmogorov–Smirnov test.

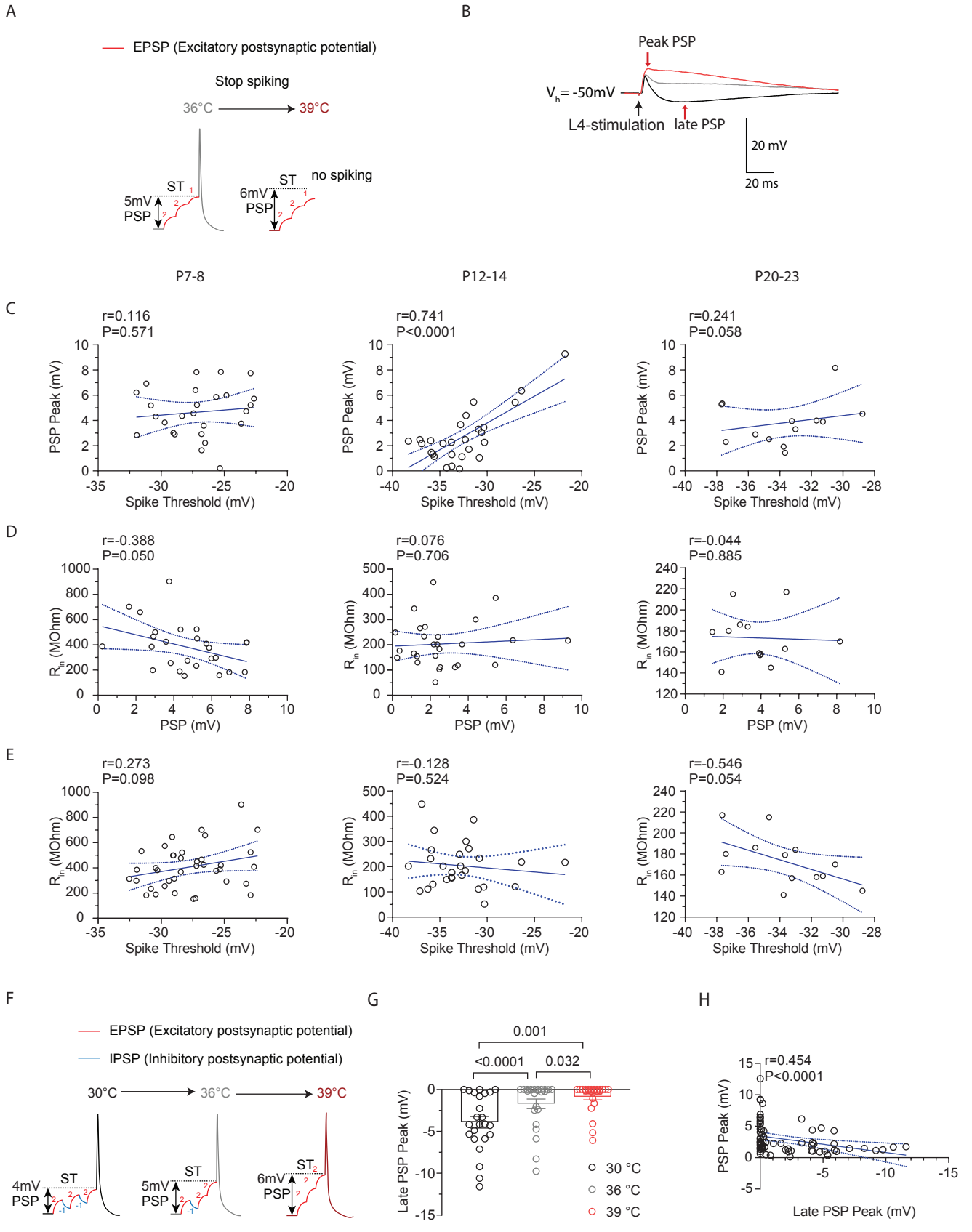

Figure 4: Increased depolarization at higher spike thresholds helps maintain stable spiking activity in cortical pyramidal neurons during temperature elevations.

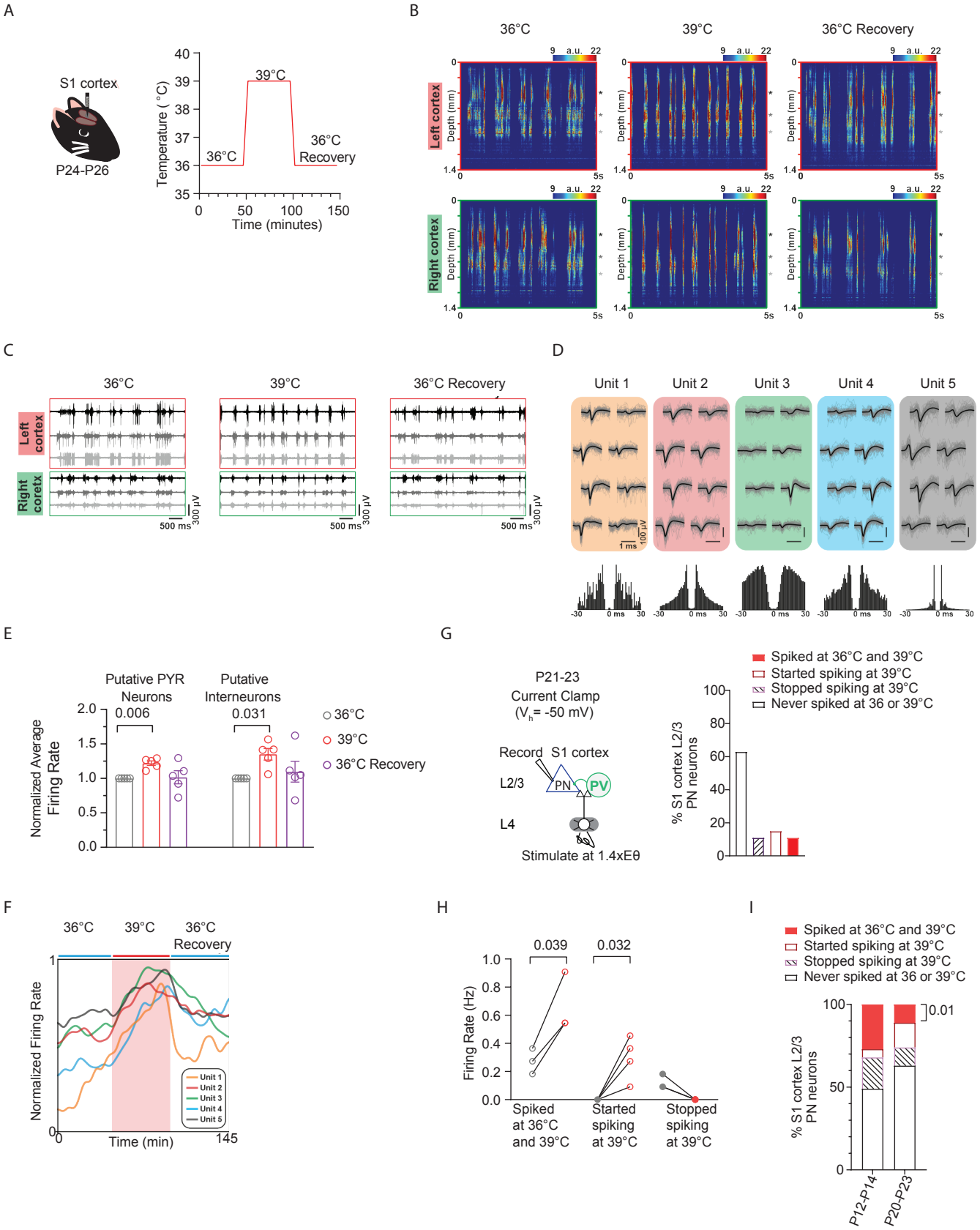

Figure 5: Cortical excitatory neurons that remain active at febrile temperatures exhibit increased spiking rates.

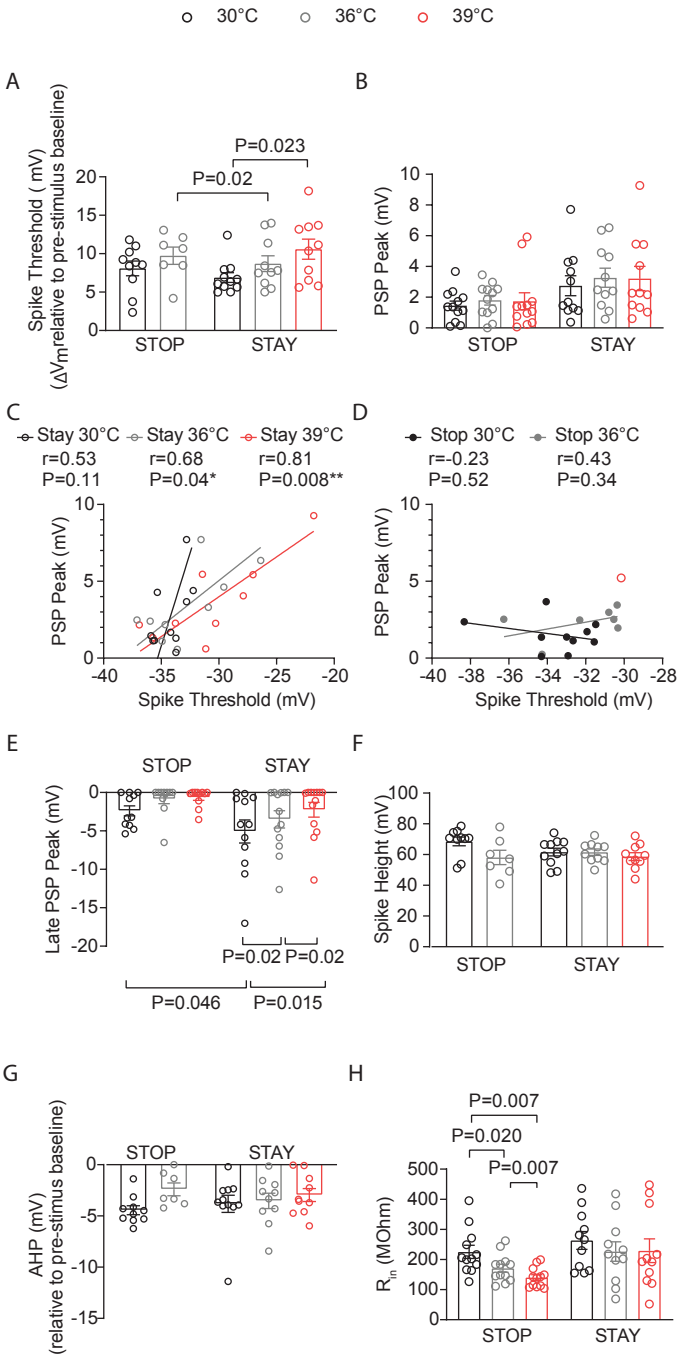

Figure 6: Excitatory pyramidal neurons that remain spiking with temperature elevations into fever range exhibit unique intrinsic properties.
Neurons that spiked at all temperatures (30°C, 36°C, and 39°C) are STAY PNs, while those that stopped spiking at 36°C or 39°C are STOP neurons.
A. Depolarization required to reach spike threshold (ST) in STOP and STAY L2/3 PNs during temperature elevations from 30°C to 39°C.
B. Same as (A) for L4-evoked postsynaptic potentials (PSPs)
C. Correlation of PSP peak versus ST in STAY L2/3 PNs at 30°C, 36°C, and 39°C. r = Pearson correlation coefficient with Deming linear regression.
D. Same as (C) for STOP cells.
E. Same as (A) for the L4-evoked late PSP peak.
F. Same as (A) for spike height.
G. Same as (A) for spike afterhyperpolarization (AHP).
H. Same as (A) for input resistance (R_{in}).
Each data point in A–H represents an individual cell. Data were collected from 14 animals. Mean ± SEM is shown in A–B and E–H. Statistical significance was assessed using one- or two-way repeated-measures ANOVA with Tukey's or Sidak post-hoc test (A–B, E–H; α = 0.05). In C–D, correlations were evaluated using Pearson's r with Deming linear regression.

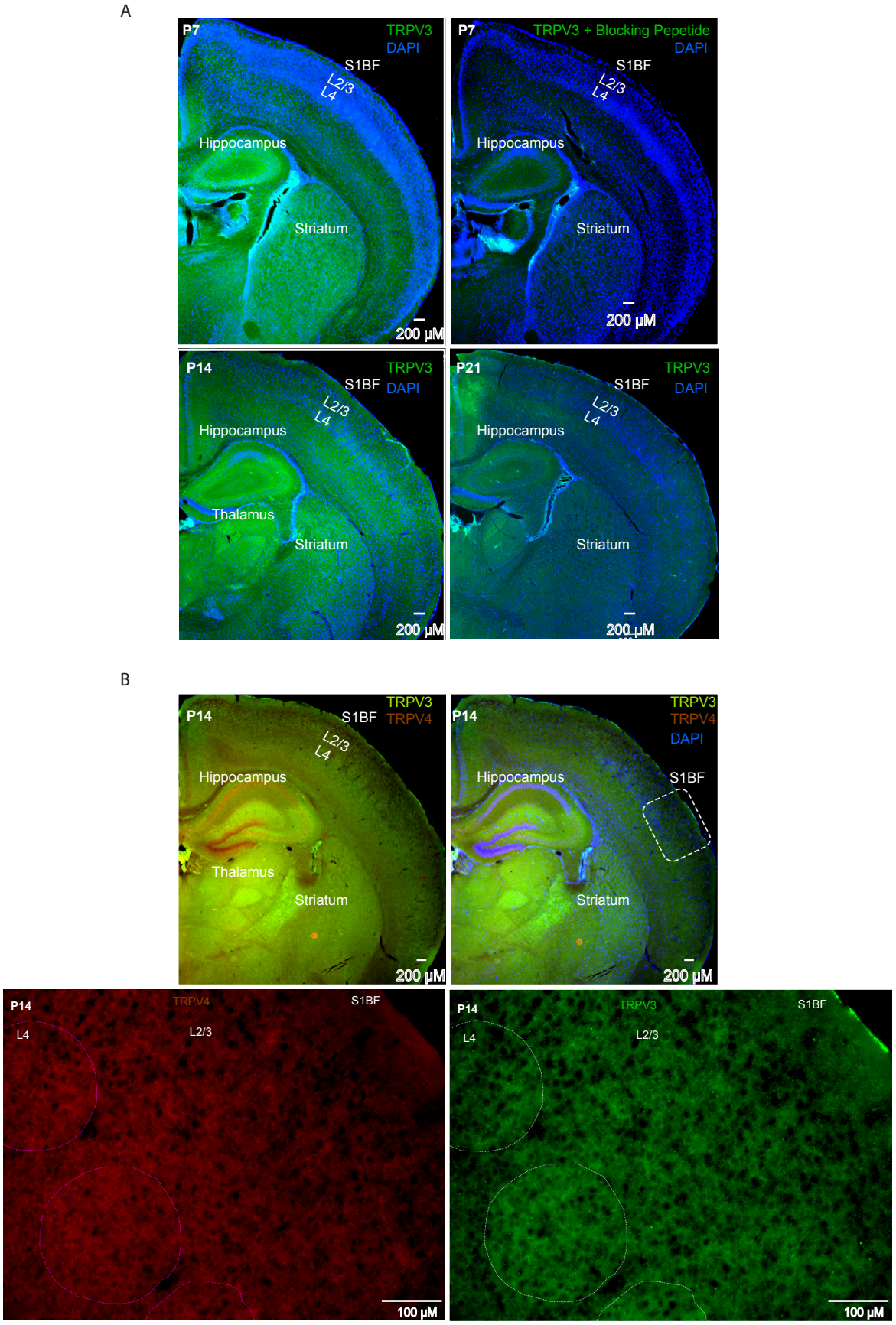

Figure 7. TRPV3 protein expression by immunohistochemistry at postnatal days 7, 14, and 21.
A. TRPV3 immunostaining (green) in mouse primary somatosensory (S1) cortex, striatum, thalamus, and hippocampus, with DAPI counterstain (blue).
Top row left: Postnatal day (P)7; bottom row left: P14; bottom row right: P21.
Top row right: Sections incubated with TRPV3 antibody plus TRPV3 blocking peptide in S1 cortex, striatum, thalamus, and hippocampus (green) with DAPI counterstain (blue). Remaining TRPV3 staining is shown in green with DAPI in blue.
B. TRPV3 and TRPV4 immunostaining in S1 cortex, striatum, thalamus, and hippocampus at P14.
Top row left: TRPV3 (green) and TRPV4 (brick red).
Top row right: TRPV3 (green) and TRPV4 (brick red) with DAPI counterstain (blue).
Bottom row left: TRPV4 immunostaining in S1BF (inset from top row left) at 10×.
Bottom row right: TRPV3 immunostaining in S1BF (inset from top row left) at 10×.

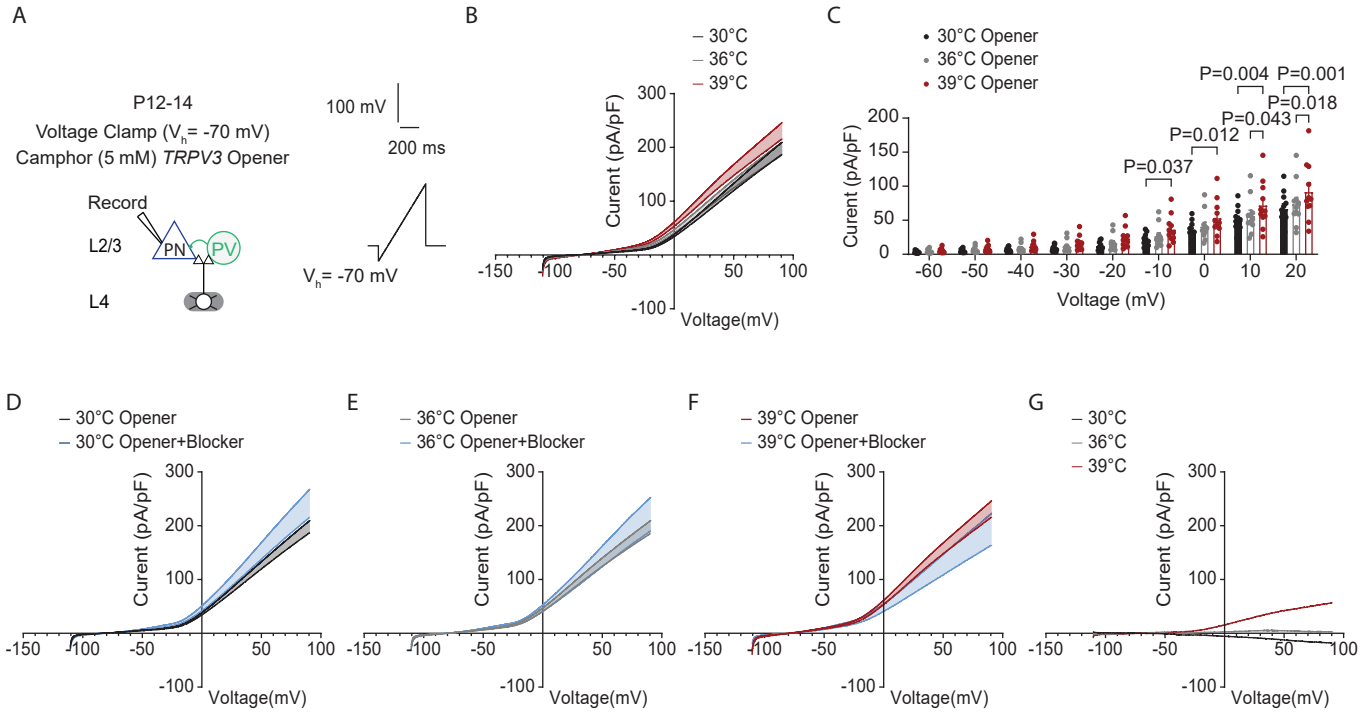

Figure 8: Temperature elevations in fever range increase TRPV3 currents in cortical pyramidal neurons.
A. Setup for recording whole-cell TRPV3 currents at 30°C (black), 36 °C (grey) and 39°C (red).
in cortical excitatory pyramidal neurons (PNs) with bath application of camphor (5mM), a TPRV3 agonist.
B. Current density-voltage (I-V) relationship of TRPV3 currents at 30°C (black), 36 °C (grey) and 39°C (red) in WT mice: 11 cells from 4 mice.
C. Scatter dot plots of the current density-voltage measurements.
D. Current density-voltage (I-V) relationship of *TRPV3* currents at 30°C (black) in the presence of camphor (5mM), a TPRV3 agonist, or camphor (5mM) + T*RPV3* blocker (Forsythoside B, 50 µM) (blue).
E. Same as (D) but for 36°C.
F. Same as (D) but for 39°C.
G. Current density-voltage (I-V) plot showing the net *TRPV3* current (opener – (opener+ blocker) condition).
In B-F, statistical significance was assessed using a two-way repeated-measures ANOVA with Tukey's or Sidak post-hoc test (α = 0.05)

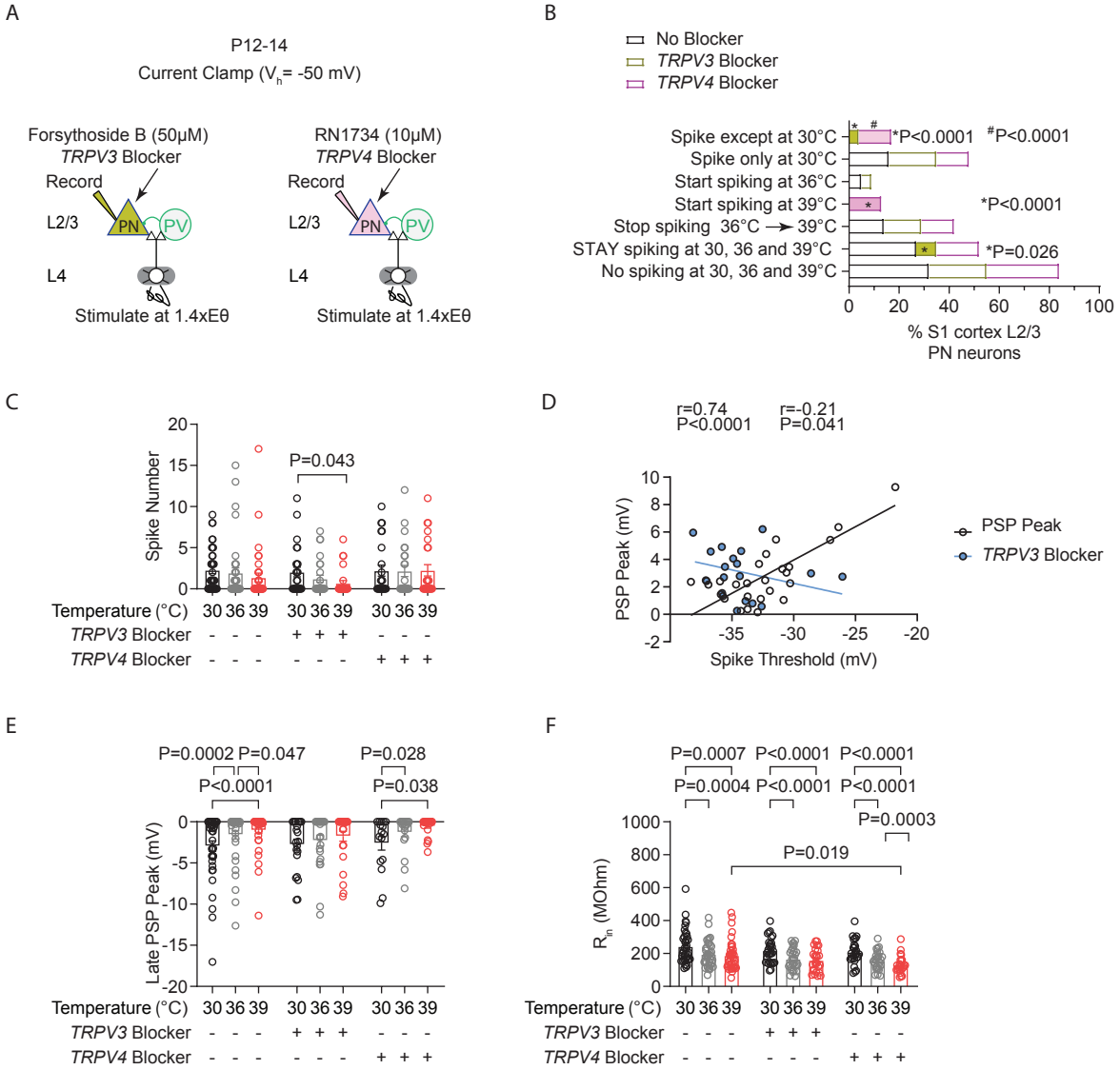

Figure 9: Inhibiting TRPV3, but not TRPV4 channels, significantly reduced the population of STAY pyramidal neurons and spiking levels at fever temperature.

A. Setup for recording L4-evoked postsynaptic potential and spiking in an excitatory cortical pyramidal neuron (PN) with an intracellular blocker of TRPV3 channels (Forsythoside B, 50 μM) (left) or TRPV4 channels (RN1734, 10 μM) (right) at just-subthreshold Vm at 30°C, 36°C, and 39°C in mouse S1 cortex.

B. Percentages of cell types obtained from experiment in A.

C. Evoked spikes in L2/3 cortical PNs during temperature elevations to 30°C, 36°C, and 39°C under three conditions: no blockers, TRPV3 blocker (Forsythoside B, 50 μM), or TRPV4 blocker (RN1734, 10 μM).

D. Correlation between PSP peak and spike threshold (ST). r = Pearson correlation coefficient with Deming linear regression.

E. Same as (C) for the L4-evoked late PSP peak.

F. Same as (C) for input resistance (R_{in}).

Each data point in C–F represents an individual cell. Data were collected from 26 cells in 7 animals for the TRPV3 blocker, 24 cells in 6 animals for the TRPV4 blocker, and 37 cells in 14 animals for the no-block condition. Mean ± SEM is shown in C, E, and F. Statistical significance was assessed using one- or two-way repeated-measures ANOVA with Tukey's or Sidak post-hoc test (α = 0.05). In D, correlations were evaluated using Pearson's r with Deming linear regression.

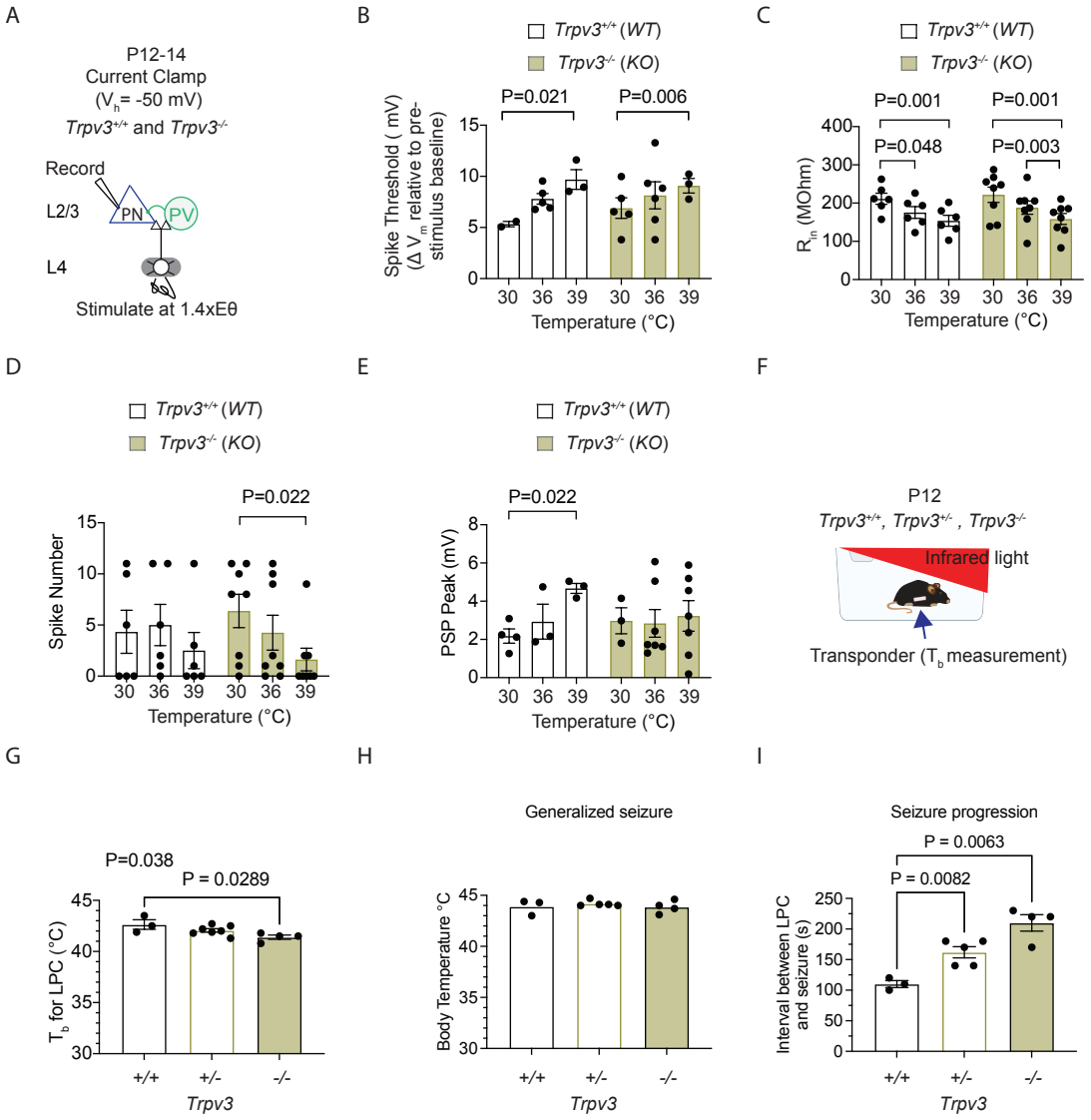

Figure 10: TRPV3 knockout mice exhibit reduced spiking activity at febrile temperatures and delayed seizure onset.
A. Setup for recording L4-evoked postsynaptic potentials and spiking in excitatory cortical pyramidal neurons (PNs) at just-subthreshold V_m at 30 °C, 36 °C, and 39 °C in mouse S1 cortex of wildtype (*Trpv3*$^{+/+}$) and Trpv3 knockout (*Trpv3*$^{-/-}$) mice.
B. Depolarization required to reach spike threshold (ST) in *Trpv3*$^{+/+}$ and *Trpv3*$^{-/-}$ mice at 30°C, 36°C, and 39°C.
C. Same as (B) but for input resistance (R_{in}).
D. Same as (B) but for number of spikes.
E. Same as (B) but for postsynaptic potential (PSP).
F. Setup for recording mouse body temperature (T_b) at room temperature and during fever-range and higher, using an implanted transponder for non-invasive measurement, with exposure to infrared light.
G. Time to loss of postural control (LPC), defined as collapse and failure to maintain upright posture, in wildtype (*Trpv3*$^{+/+}$), heterozygous (*Trpv3*$^{+/-}$) and Trpv3 knockout (*Trpv3*$^{-/-}$) mice.
H. Same as in (G) but showing T_b at seizure onset.
I. Same as in (G) but for the time from LPC to seizure onset.
Each data point in B–E represents an individual cell (3 animals per genotype). Statistical significance was assessed using two-way repeated-measures ANOVA with Tukey's or Sidak post-hoc test (α = 0.05). Each data point in G–I represents an individual animal. Statistical significance was assessed using one-way repeated-measures ANOVA with Tukey's or Sidak post-hoc test (α = 0.05).

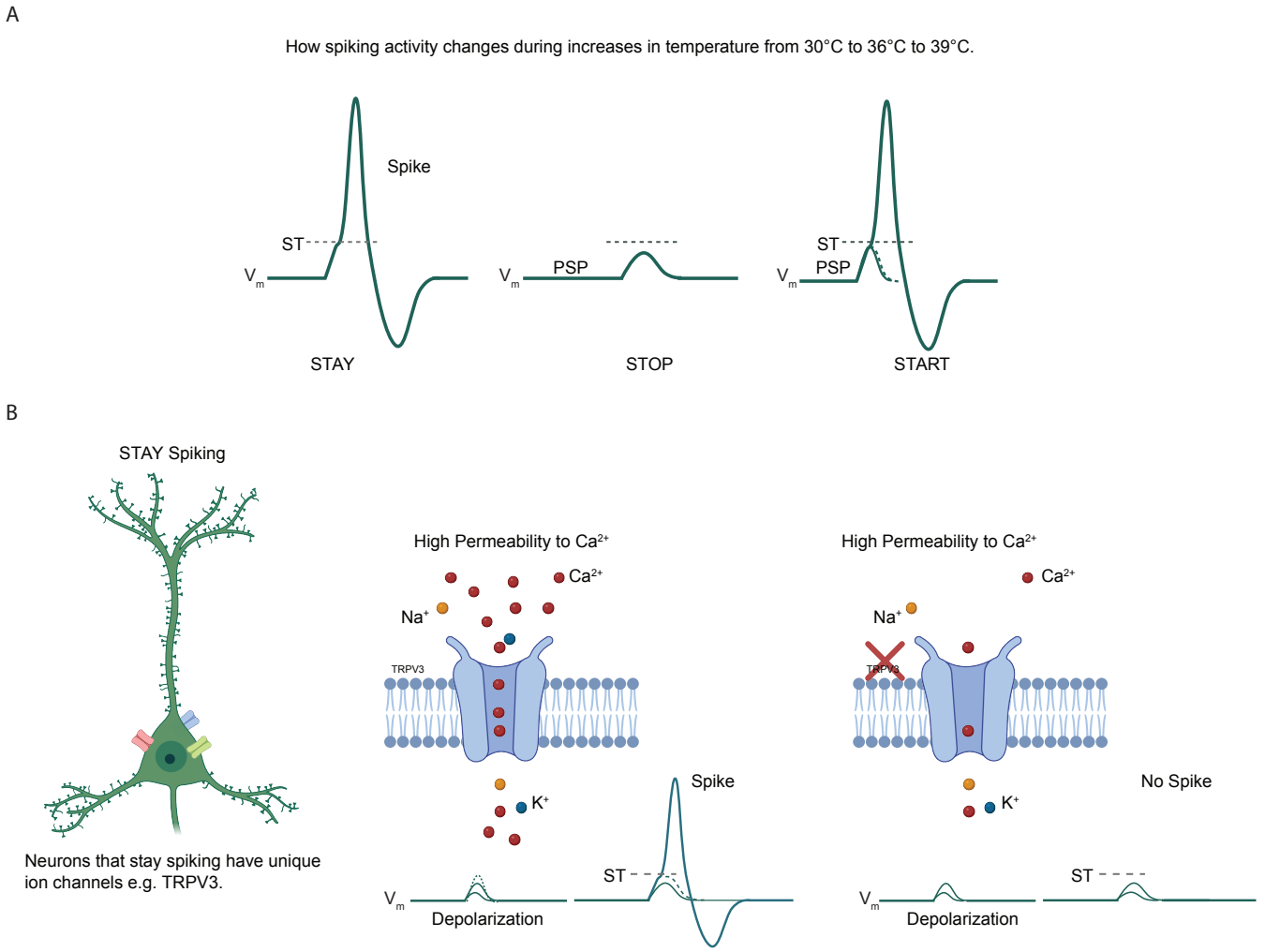

Figure 11. Summary model of how STAY neurons achieve firing stability through unique ion channel compositions, including TRPV3.
A. In cortical L2/3 pyramidal neurons (PNs) with synaptically evoked spiking, gradual increases in brain slice temperature from 30 °C to 36 °C to 39 °C result in four possible outcomes: neurons remain inactive, continue spiking (STAY), stop spiking, or initiate spiking.
To spike, PNs must reach spike threshold (ST), defined as the minimal Vm that elicits an action potential, which requires sufficient depolarization via the postsynaptic potential (PSP). STAY neurons consistently reach ST and continue spiking. Neurons that stop spiking fall below the level of depolarization required to reach ST, while neurons that initiate spiking achieve sufficient depolarization to newly reach ST.
B. STAY neurons may contain unique ion channels, such as TRPV3. TRPV3 channels are highly permeable to Ca^{2+} ions, and Ca^{2+} influx contributes to PN depolarization. The presence of TRPV3 facilitates greater ion entry, enabling depolarization sufficient to reach ST and sustain spiking, whereas its absence reduces depolarization to levels insufficient for spiking.